

# Does increased spatial replication above heterogeneous agroforestry improve the representativeness of eddy covariance measurements?

José Ángel Callejas-Rodelas<sup>1</sup>, Alexander Knohl<sup>1,2</sup>, Ivan Mammarella<sup>3</sup>, Timo Vesala<sup>3,4</sup>, Olli Peltola<sup>5</sup>, and Christian Markwitz<sup>1</sup>

<sup>1</sup>University of Göttingen, Bioclimatology, Göttingen, Germany

<sup>2</sup>Centre for Biodiversity and Land Use, University of Göttingen, Göttingen, Germany

<sup>3</sup>Institute for Atmosphere and Earth System Research (INAR)/Physics, Faculty of Science, University of Helsinki

<sup>4</sup>Institute for Atmosphere and Earth System Research (INAR)/Forest Science, Faculty of Agriculture and Forestry, University of Helsinki

<sup>5</sup>Natural Resources Institute Finland (LUKE), Latokartanonkaari 9, Helsinki, 00790, Finland

**Correspondence:** José Ángel Callejas-Rodelas (joseangel.callejasrodelas@uni-goettingen.de)

1 **Abstract.** Spatial heterogeneity in terrestrial ecosystems compromises the accuracy of eddy covariance measurements. ~~An~~  
2 ~~example~~ Examples of heterogeneous ecosystems are temperate agroforestry systems, that have been poorly studied by eddy  
3 covariance. Agroforestry systems get an increasing attention due to their potential environmental benefits, e.g. a higher carbon  
4 sequestration, ~~enhanced~~ improved microclimate and erosion reduction compared to ~~monocropping~~ open cropland agricultural  
5 systems. Lower-cost eddy covariance setups might offer an opportunity to ~~reduce this bias~~ better capture spatial heterogeneity  
6 by allowing for more spatial replicates of flux towers. The aim of this study was to quantify the spatial variability of carbon  
7 dioxide (*FC*), latent heat (*LE*) and sensible heat (*H*) fluxes above a heterogeneous agroforestry system in northern Germany  
8 using a distributed network of three lower-cost eddy covariance setups across the agroforestry systems. Fluxes from the three  
9 towers in the agroforestry were further compared to fluxes from an adjacent ~~monocropping~~ open cropland site. The campaign  
10 took place from March 2023 until September 2024. The results indicated that the spatial variability of fluxes was largest for  
11 *FC*, attributed to the effect of different crops (rapeseed, corn and barley) within the flux footprints ~~contributed~~ contributing  
12 to the measured fluxes. Differences between fluxes across towers were enhanced after harvest events. However, the temporal  
13 variability due to the seasonality and diurnal cycles during the campaign was larger than the spatial variability across the three  
14 towers. When comparing fluxes between the agroforestry and the ~~monocropping~~ open cropland systems, weekly sums of carbon  
15 and evapotranspiration fluxes followed similar seasonality, with peak values ~~during the growing season~~ of  $-50 \text{ g C m}^{-2} \text{ week}^{-1}$   
16 and  $40 \text{ mm week}^{-1}$  during the growing season, respectively. The variation of the magnitude depended on the phenology of the  
17 different crops. The effect size, which is an indicator of the representativeness of the fluxes across the distributed network of  
18 three eddy covariance towers against only one, showed in conjunction with the other results that the spatial heterogeneity across  
19 the agroforestry was better captured by the network of three stations. This supports previous findings that spatial heterogeneity  
20 should be taken into account in eddy covariance studies, and that lower-cost setups may offer the opportunity to bridge this gap  
21 and improve the accuracy of eddy covariance measurements above heterogeneous ecosystems.

## 22 1 Introduction

23 The eddy covariance (EC) technique is the central approach to measuring the exchange of energy, trace gases and momen-  
24 tum between terrestrial ecosystems and the atmosphere (??)(Baldocchi, 2014). The EC technique has been established as a  
25 standard method within the scientific community when rapid-response instruments, capable of measuring wind speed, tem-  
26 perature, and gas concentrations over the major frequency ranges of the turbulent energy spectrum became commercially  
27 available (??)(Aubinet et al., 2012; Wohlfahrt et al., 2009). These instruments provided the capability to measure the exchange  
28 of energy and matter between the land surface and the atmosphere, driven by eddies of diverse sizes and frequencies (??  
29 (Kaimal and Finnigan, 1994).

30 At a majority of flux sites, a single EC station is installed (??)(Hill et al., 2017) and measurements are made based on the  
31 ergodic hypothesis. The ergodic hypothesis states that covariances (fluxes) calculated over the time domain are equivalent to  
32 covariances calculated over the spatial domain (??)(Higgins et al., 2013). The measured turbulent fluxes and carbon and water  
33 balances, when integrated over a defined time interval, are representative of the tower footprint area corresponding to the  
34 averaging interval (??)(Vesala et al., 2008). This is true for homogeneous sites where the spatial representativeness of fluxes  
35 within the ecosystem of interest is guaranteed with a high degree of confidence (??)(Hurlbert, 1984). However, these conditions  
36 of homogeneity are often not met in many ecologically and socioeconomically interesting sites, such as mixed forests, wetlands,  
37 urban forest interfaces or small-scale farmlands (??)(Finnigan et al., 2003; Hill et al., 2017).

38 Agroforestry (AF) systems are an example of heterogeneous agroecosystems. They combine trees and crops on the same  
39 agricultural land in order to benefit from the presence of trees on the land (??)(Veldkamp et al., 2023; Kay et al., 2019). These  
40 systems offer several benefits, including the potential to prevent wind erosion over crops (??)(van Ramshorst et al., 2022; Böhm et al., 2014  
41 , improve soil fertility (??)(Kanzler et al., 2021), or reduce water loss through evaporation in crops (??)(Kanzler et al., 2019).  
42 Short Rotation Alley Cropping systems, a type of agroforestry, represent an alternative land use practice with the potential to  
43 increase carbon sequestration and improve water use efficiency (WUE) in comparison to conventional ~~monocropping (MC)~~  
44 ~~agriculture~~ (??) ~~open cropland (OC)~~ agriculture (Markwitz et al., 2020; Veldkamp et al., 2023). These AF systems consist of  
45 alternating rows of trees and crops. The trees employed in these systems are typically fast-growing species, such as poplar  
46 (*Populus*) or willow (*Salix*), and are harvested in cycles of 5-6 years for biomass production. Crops are cultivated in an annual  
47 rotation.

48 ~~The spatial configuration of the AF system influences the wind flow regimes within the ecosystem, thereby affecting the~~  
49 ~~development of turbulence. In many cases~~ In general, heterogeneity poses a challenge for EC measurements and, in a broader  
50 context, for any type of measurement across the atmospheric boundary layer (Bou-Zeid et al., 2020). Heterogeneity in surface  
51 properties induces horizontal advection, secondary mesoscale circulations and non-equilibrium turbulence processes, which  
52 occur near and downstream of changes in the surface properties (Bou-Zeid et al., 2020). As shown by previous studies over  
53 heterogeneous sites, such as ~~over-tall vegetation, EC measurements are made within the roughness sub-layer (RSL), which~~  
54 ~~is, by definition, the atmospheric layer whose dynamics are influenced by the roughness elements and is located below the~~  
55 ~~inertial sub-layer (?). At the AF, the trees act as an effective wind barrier (?), thus modifying the RSL, creating internal~~

boundary layers (?), and changing the characteristics of turbulence over the field. In addition, the alternation of trees and crops with differing phenologies and canopy heights creates a heterogeneous distribution of carbon and water vapor sources and sinks. This spatial variability is likely to have an impact on the measured fluxes, as shown by other authors who have studied the spatial variability of fluxes over different ecosystems, such as pine forest (??) or managed grassland (?) pine forest (Katul et al., 1999; Oren et al., 2006) or managed grassland (Peltola et al., 2015), spatial heterogeneity induced relevant spatial variability in the EC measured fluxes. According to the classification of Bou-Zeid et al. (2020), the heterogeneity of these AF systems can be classified as unstructured heterogeneity (Fig. 1 therein), because the site consists of a certain number of interleaved trees and crop strips, but it is small enough that the AF site might be affected by other elements in the surrounding landscape. Upon changes in surface properties (like roughness or moisture), the mean wind field and the turbulence adjust to the new surface, with more complex effects on the flow when multiple changes in the surface properties co-occur, as it is the case at the AF (Bou-Zeid et al., 2020).

The location of the EC station within a land use system has been demonstrated to potentially introduce a bias in the measured fluxes (?) (Chen et al., 2011), indicating that a single EC station may not be sufficient to properly account for the spatial variability of fluxes induced by landscape heterogeneity (?) (Katul et al., 1999). The high cost and labor intensity of deploying an EC station are the main reasons for the lack of spatial replicates of EC measurements in many studies (?) (Hill et al., 2017). The infrared gas analyzer (IRGA), the crucial component to measure trace gases, typically accounts for a large proportion of the total installation costs associated with an EC station. Lower-cost EC (LC-EC) setups represent a potential solution to the spatial replication problem of EC measurements, as several EC stations could be deployed for the cost of a single conventional station. LC-EC employ a more economical infrared gas analyser and a sonic anemometer, though these instruments necessitate more rigorous post-processing corrections. Notably, previous studies have demonstrated that LC-EC setup can yield comparable results to those of conventional EC (CON-EC) setups. ? Hill et al. (2017) compared a custom-built LC-EC setup for CO<sub>2</sub> and H<sub>2</sub>O measurements with a CON-EC, with very good agreement in CO<sub>2</sub> and H<sub>2</sub>O fluxes. In addition, a different LC-EC setup for H<sub>2</sub>O flux measurements was compared with a conventional setup ? (Markwitz and Siebicke, 2019), resulting in good agreement in H<sub>2</sub>O fluxes. Furthermore, another version of the LC-EC setup deployed in ? Hill et al. (2017) was extensively validated in the studies of ? and ? Callejas-Rodelas et al. (2024) and van Ramshorst et al. (2024), with very good agreement in CO<sub>2</sub> fluxes and good agreement in H<sub>2</sub>O fluxes.

The LC-EC setups can allow for a higher degree of spatial replication of EC and support conventional EC setups. In addition, they provide a powerful tool for the verification of carbon and water balances in the agricultural and forestry sectors in developing carbon credit markets (?) (Trouwloon et al., 2023) or for an improved water management. However, the increased uncertainty associated with these setups must be taken into account when calculating balances of energy, carbon, or other variables, and when comparing different land uses. One of the main differences between LC-EC and CON-EC setups is the spectral response of the sensors. The LC-EC setups used in the ?, ?, ? and ? Callejas-Rodelas et al. (2024), Cunliffe et al. (2022), Hill et al. (2017) and van Ramshorst et al. (2024) studies were characterized by a slower frequency response in CO<sub>2</sub> and H<sub>2</sub>O measurements, which induces a higher spectral attenuation in the high-frequency range of the turbulent energy spectrum, com-

pared to CON-EC. The higher attenuation introduces a greater degree of uncertainty when applying spectral corrections, as observed by ~~?~~ and ~~?~~ [Ibrom et al. \(2007\)](#) and [Mammarella et al. \(2009\)](#), among others.

The impact of landscape heterogeneity within ~~a~~-an AF system on turbulence, latent heat flux ( $LE$ ), sensible heat flux ( $H$ ) and carbon dioxide flux ( $FC$ ) remains to be examined. ~~?~~ and ~~?~~ [Markwitz and Siebicke \(2019\)](#) and [Markwitz et al. \(2020\)](#) conducted evapotranspiration ( $ET$ ) measurements across multiple AF and ~~MC~~-~~OC~~ systems in Northern Germany; however, their measurements were not replicated within a single site. In contrast, in the study of ~~?~~ [Cunliffe et al. \(2022\)](#) a total of eight LC-EC setups were deployed in different locations across a landscape of ecological interest (~~?~~) [\(Cunliffe et al., 2022\)](#). The objective of this study was to capture the heterogeneity of ~~CO<sub>2</sub>~~-~~FC~~ and  $ET$  fluxes across a semiarid ecosystem, with low magnitude of both ~~CO<sub>2</sub>~~-~~FC~~ and  $ET$  fluxes. ~~To the best of our knowledge, replicated.~~ [Replicated EC](#) measurements in heterogeneous agroforestry systems are so far lacking.

In the present study, a network of three LC-EC setups was deployed, analogous to those utilized in the studies of ~~?~~, ~~?~~ and ~~?~~ [Callejas-Rodelas et al. \(2024\)](#), [Cunliffe et al. \(2022\)](#) and [van Ramshorst et al. \(2024\)](#), above an AF site, and one additional LC-EC setup above an adjacent ~~MC~~-~~OC~~ site in northern Germany. To the best of our knowledge, this was the first time a distributed network of EC towers has been installed above a temperate agroforestry system. With one and a half years of concomitant flux data from the four EC setups, the objective was to quantify the spatial and temporal variability of  $FC$  and  $LE$ , as well as the statistical effect of the increased spatial replication of EC measurements above a heterogeneous site. According to ~~?~~ [Hill et al. \(2017\)](#), it is possible to estimate the sampling variability and total uncertainty for an ecosystem with independent spatial replication of EC measurements. This allows for the estimation of the effect size (see Section 2). The present study tested the hypothesis that the increased uncertainty inherent to the use of slower-frequency response sensors in EC measurements can be counteracted by the improvement of spatial replication of EC, which increases its statistical robustness. The objectives of this study were threefold: (i) to quantify the spatial and temporal variability of turbulent fluxes and parameters above AF; (ii) to calculate the effect size of the experimental site ~~,~~ following ~~?~~ [at the daily scale, following Hill et al. \(2017\)](#); and (iii) to compare the ecological functioning of the AF to the ~~MC~~-~~OC~~ in terms of ~~carbon~~-~~FC~~ and  $ET$  balances.

## 2 Methods

### 2.1 Site description

The measurements were conducted from 1 March 2023 to 19 September 2024 at an agroforestry system located in Wendhausen (Lehre), Lower Saxony, Germany (52.63° N, 10.63° E). Elevation above sea level is 80 m. The field is divided into two distinct systems: an AF system ([17.3 ha](#)) in the north and a ~~MC~~-~~system~~-~~OC~~ system ([8.5 ha](#)) in the south (see Fig. 1). The ~~AF-system~~ ~~covers an area of 17.3 ha and the MC covers an area of 8.5 ha. The~~ crops cultivated within both systems kept a similar distribution from west to east. In 2023, rapeseed was cultivated at the western side, barley at the eastern side, and corn at the center (Fig. 1a). In 2024, rapeseed was cultivated at the eastern side, barley at the center, and corn at the western side (Fig. 1b). The management of the crops was similar at both AF and ~~MC~~-~~OC~~ sites and crops were fertilized. The mean long-term annual precipitation is 617 mm, and the mean annual air temperature is 9.9 °C, for the reference period 1981-2010 at Braunschweig



123 airport ((?)[\(DWD, 2024\)](#)). The soil at both AF and [MC-OC](#) sites was classified as a Clay Cambisol, with an organic carbon  
 124 (SOC) content of 5.8 kg C m<sup>-2</sup> at the [MC-OC](#) and and 6.75 kg C m<sup>-2</sup> at the AF. Additionally, the soil bulk density was  
 125 determined as 1.0 g cm<sup>-3</sup> at both AF and [MC\(?\)OC](#) ([Veldkamp et al., 2023](#)). Soil characteristic were last measured in 2019.  
 126 The harvest of rapeseed, barley and corn in the 2023 campaign season occurred on 13 July, 22 August and 26 and Septem-  
 127 ber. The harvest of rapeseed, barley and corn in the campaign of 2024 took place on 15 July, 5 August and 13 September,  
 128 respectively. In 2024, rapeseed did not grow well and a mulch cut was carried out, therefore the eastern part of the field was  
 129 covered by a combination of grasses, bare soil and mulch. Canopy height was estimated from pictures taken during field visits.  
 130 The maximum height attained by the crops at the peak of their development stage was around 1.5 m for rapeseed, 2.5 m for  
 131 corn and 1.3 m for barley. The trees present at the AF system are fast-growing poplar (*Populus nigra* × *Populus maximowiczii*)  
 132 and are typically harvested every 4 to 5 years. The most recent [harvest-of-these-trees-tree harvest](#) occurred in 2019. Trees grew  
 133 from around 4.0 m till 5.5 m on average across the measurement period. [Further details on the site are provided in ?.](#)

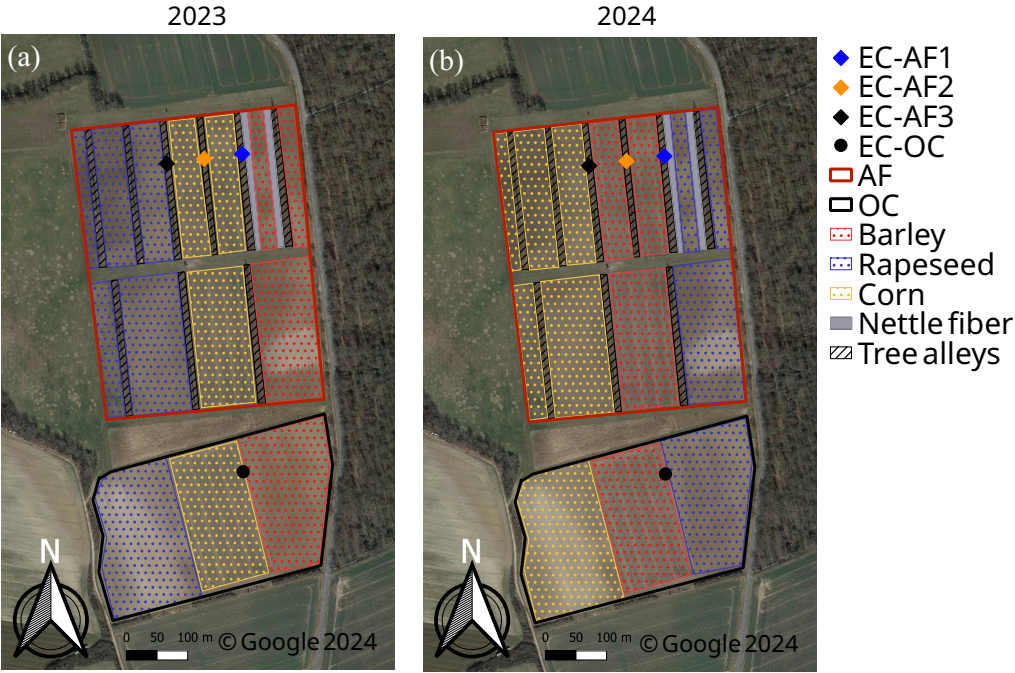


**Figure 1.** Satellite view and land cover classification of the experimental site for 2023 (a) and 2024 (b), together with the location of the EC stations (blue diamond for EC-AF1, orange diamond for EC-AF2, black diamond for EC-AF3 and black circle for [EC-MC-OC](#)). The area bordered red corresponds to the AF system and the area bordered blue to the [MC-OC](#) system. Figure created with QGIS v. 3.22, aerial map by Google Satellite Maps. © Google 2024.

## 134 2.2 Experimental setup

135 Measurements were made at four EC stations, one located at the [MC-OC](#) site and three located at the AF site (Fig. 1). The  
 136 stations are designated as [MC-OC](#), AF1, AF2 and AF3. Each station was equipped with a complete set of meteorological sensors

137 and a LC-EC setup (see Table 1 in [Callejas-Rodelas et al., 2024](#)). The measured meteorological variables were air temperature  
138 (*TA*), relative humidity (*RH*), atmospheric pressure (*PA*), precipitation (*P*), global radiation (*SW\_IN*), outgoing shortwave  
139 (*SW\_OUT*) and longwave ~~radiation~~ (*LW\_OUT*) [radiation](#), and net radiation (*NETRAD*). The EC measurement heights were 10  
140 m above ground for AF1, AF2 and AF3, and 3.5 m for [MEOC](#). Only one photosynthetic active radiation (*PPFD\_IN*) sensor  
141 was installed at AF1, and two barometers for atmospheric pressure measurements were installed at AF1 and AF2. All the  
142 stations were equipped with two soil heat flux plates to measure soil heat flux (*G*) at 5 cm depth. Only one soil heat flux plate  
143 was installed at AF3. Radiation sensors were placed in a beam facing south at ~~9-9.5~~ m height at AF1, AF2 and AF3 and at  
144 3 m height at [MEOC](#). *TA* and *RH* measurements were taken at 2 m height at all stations. [P was measured at 1 \(AF1, OC\) or](#)  
145 [1.5 \(AF2, AF3\) m height](#). Meteorological data were recorded on CR1000X dataloggers (Campbell Scientific Inc., Logan, UT,  
146 USA).

147 The LC-EC setups consisted of a three-dimensional sonic anemometer for wind measurements (uSonic3-Omni, METEK  
148 GmbH, Elmshorn, Germany) and a gas analyzer enclosure. The enclosure consisted of an IRGA for CO<sub>2</sub> ~~mole-fraction-molar~~  
149 [density](#) measurements (GMP343, Vaisala Oyj, Helsinki, Finland), and a *RH* capacitance cell for *RH* measurements (HIH-4000,  
150 Honeywell International Inc., Charlotte, North Carolina, USA) and was installed at the bottom of the tower. Air was drawn  
151 through a 9 m tube at the AF stations and 2.5 m tube at the ~~MC-OC~~ station. Two temperature sensors were installed, one inside  
152 the IRGA measuring cell and one inside the enclosure; and two pressure sensors, one to measure differential pressure inside the  
153 enclosure and another to measure absolute pressure inside the IRGA measuring cell. Measurements from all components were  
154 recorded at 2 Hz frequency on a CR6 datalogger (Campbell Scientific Inc., Logan, UT, USA). A more detailed description of  
155 the setup can be found in [Callejas-Rodelas et al. \(2024\)](#).

156 The GMP343 sensors were calibrated in February 2023 and February 2024. Frequent inspections were performed to clean  
157 the tubing, replace filters, measure flow rate, and clean the lens of the GMP343. The nominal flow rate was 5.0 L·min<sup>-1</sup> at  
158 all AF stations, with some drops due to filter clogging, ~~and 2.2 L·min<sup>-1</sup> at the MC before March 14<sup>th</sup> 2023 and 5.0 L·min<sup>-1</sup>~~  
159 ~~thereafter, due to the replacement of the pump by a more powerful one.~~

160 During the study period, there were generally large percentages of missing data. Missing data were either short gaps (a few  
161 30-minute periods or a few hours) caused by data filtering during the quality control after flux processing (see Section 2.3.3), or  
162 longer gaps (hours to a few days) due to power outages during the winter, mostly at night, at all stations. Due to other technical  
163 problems, there were few larger gaps at some stations, in particular a gap of three months from mid-July to early October 2023  
164 at AF3, for *FC* and *LE*.

165 Although generally recommended in EC studies ~~(?)~~ [\(Aubinet et al., 2012\)](#), no storage terms were considered in the calcula-  
166 tion of *FC* and *LE* because no concentration profiles were installed at the stations.

## 167 2.3 Flux computation

### 168 2.3.1 Pre-processing

169 Data processing prior to flux calculation included (i) the calculation of CO<sub>2</sub> dry mole fraction measurements from the CO<sub>2</sub>  
170 molar density provided by default by the instrument, using some sensor-specific parameters and the observed values of pressure  
171 and relative humidity in the measurement system ~~(?)~~([Callejas-Rodelas et al., 2024](#)); and (ii) the calculation of the H<sub>2</sub>O dry mole  
172 fraction from relative humidity, temperature and pressure measurements inside the measurement cell using the derivation of ~~?~~  
173 [Markwitz and Siebicke \(2019\)](#). More details on the pre-processing steps are given in ~~?~~~~and ?~~[Callejas-Rodelas et al. \(2024\)](#) and  
174 [van Ramshorst et al. \(2024\)](#).

### 175 2.3.2 Flux processing

176 *H*, *LE*, *FC* and momentum flux were calculated using the EddyUH software ~~(?)~~([Mammarella et al., 2016](#)) in its Matlab version  
177 (MATLAB®R2023a, The Mathworks, Inc., Natick, MA, USA). Raw data were de-spiked using limits for absolute differences  
178 between consecutive values. Detrending was performed by block averaging. Wind coordinates were binned into eight sec-  
179 tors [of 45° each](#) and rotated according to the planar fit correction procedure of [?Wilczak et al. \(2001\)](#), [following the default](#)  
180 [recommendation by ICOS \(Sabbatini et al., 2018\)](#). Time-lag optimization was performed through cross-covariance maximiza-  
181 tion, using predefined windows of 2 to 10 s for CO<sub>2</sub> and 2 to 20 s for H<sub>2</sub>O ~~(?)~~([Callejas-Rodelas et al., 2024](#)). Low-frequency  
182 losses were corrected after [?Rannik and Vesala \(1999\)](#) and high-frequency losses~~after ?~~, [after Mammarella et al. \(2009\)](#). The  
183 latter is based on ~~the determination of the~~ [determining the](#) time response of CO<sub>2</sub> and H<sub>2</sub>O separately, calculated from [the](#)  
184 measured co-spectra. In the case of CO<sub>2</sub> the time response determined by the experimental method was similar to the nominal  
185 time response of 1.36 s calculated in [?Hill et al. \(2017\)](#) for the GMP343. This time response was used for all flux calculations  
186 for all the ~~three-four~~ towers. In the case of H<sub>2</sub>O the time response was estimated by a exponential fit as a function of relative  
187 humidity. Data quality was flagged from 1 to 9 following [?Foken et al. \(2005\)](#).

### 188 2.3.3 Filtering and gap filling

189 Fluxes were filtered using data with quality flags < 7 to avoid periods with poorly developed turbulence ~~(?)~~([Foken et al., 2005](#)).  
190 Outliers were removed using a running median absolute deviation (MAD) filter, based on the approach by [?Mauder et al. \(2013\)](#)  
191 , with a window of two weeks. The *q* parameter in Eq. (1) of the paper by [?Mauder et al. \(2013\)](#) was set as 7.5. The MAD filter  
192 was iterated three times over each time series. Hard upper and lower limits were applied afterwards to remove ~~any~~-additional  
193 outliers not detected by the MAD filter. Values outside the ranges from -100 W m<sup>-2</sup> to 700 W m<sup>-2</sup> for *H*, from -20 W m<sup>-2</sup> to  
194 700 W m<sup>-2</sup> for *LE*, and from ~~-55-50~~ μmol m<sup>-2</sup> s<sup>-1</sup> to ~~55-50~~ μmol m<sup>-2</sup> s<sup>-1</sup> for *FC*, were discarded. Additional hard limits  
195 were applied specifically to winter (November to February) and transition periods (March and October) separately. The aim  
196 was to avoid outliers that went through the previous filters which might bias the application of the gap-filling algorithms. For  
197 *LE* and *H*, these limits were of 50 W m<sup>-2</sup> during winter, and 100 W m<sup>-2</sup> in March and October. For the *FC*, these limits were

(in absolute values)  $\pm 10 \mu\text{mol m}^{-2} \text{s}^{-1}$  during winter, and  $\pm 15 \mu\text{mol m}^{-2} \text{s}^{-1}$  in March and October. Finally, a friction velocity (*USTAR*,  $\text{m s}^{-1}$ ) filter was applied to remove periods with non-existent or weak turbulence. The filter of *USTAR* was applied using REdDyProc (?) (Wutzler et al., 2018), which removed values based on a *USTAR* threshold calculated as the maximum of the seasonally derived *USTAR* values. These seasonal values were calculated based on ?Papale et al. (2006). The average *USTAR* thresholds for the stations were 0.21, 0.21, 0.18 and 0.16  $\text{m s}^{-1}$  for AF1, AF2, AF3 and MCOC, respectively. The-Before filtering, the total available data before-filtering accounted for 63.4 % (AF1), 80.0 % (AF2), 76.2 % (AF3) and 61.5 % (MCOC) for *FC* and *LE*, respectively, and 85.7 % (AF1), 86.0 % (AF2), 83.1 % (AF3) and 75.9 % (MCOC) for *H*, respectively, relative to the duration of the whole-entire measurement campaign. These gaps were-occurred due to instrumental or power failure. After filtering, the available data accounted for 36.5-39.3 % (AF1), 44.8-49.2 % (AF2), 31.3-35.7 % (AF3) and 29.2 %- (MC33.8 % (OC), for *FC*; 41.6-42.0 % (AF1), 50.1-53.6 % (AF2), 36.1-36.4 % (AF3) and 38.5 %- (MC38.7 % (OC) for *LE*; and 61.4-61.5 % (AF1), 60.0-61.4 % (AF2), 56.4-56.7 % (AF3) and 52.3 %- (MC52.8 % (OC) for *H*. Additional gaps in filtered data were introduced by rejecting data-

Meteorological data were gap-filled at the 30-minute time scale in-order to provide complete time series for-the-variables acting-as-predictors-for-the-of-the-predictor-variables-for flux gap-filling-,with-slight-differences-in-the-procedure-. The procedure differed slightly for the different variables of interest. Short gaps of up to one hour were filled using linear interpolation, except for *P*. Missing data at the AF1 stationthat-were-, when available at the MC-OC station, were filled using linear regression models using-as-predictors-the-data-from-the-MC-,and-viceversa-with-the-OC-data-as-predictors-,and-vice-versa. Missing data at AF2 and AF3 -,but-that-were available at AF1 -,were filled using a similar procedure, with AF1 as the reference. Finally, *P*, *TA*, *RH*, vapor pressure deficit (*VPD*), *SW\_IN*, wind speed (*WS*) and wind direction (*WD*) were filled at the stations using ERA5-Land re-analysis data (?) (Muñoz-Sabater et al., 2021) as predictors, following the approach implemented in ?-Linear Vuichard and Papale (2015). Linear reduced major axis regression models were derived from the ERA5-Land data and the station data, using the library *pylr2* in Python. The coefficients (slope and intercept) from the linear models were then used to calculate the missing values. *PPFD\_IN* was filled based on global radiation (*SW\_IN*), by multiplying *SW\_IN* by the average ratio between *PPFD\_IN* and *SW\_IN* for the available periods at the site. *P* was filled by multiplying the ERA5-Land data by the ratio between the station data and the re-analysis data, as done-in-?-Possible-in Vuichard and Papale (2015). Any inaccuracies resulting from this replacement did not contribute-to-an-introduce additional bias in the gap-filled flux time series -,as-because precipitation was not used for gap-fillingpurposes. A quality flag was developed-for-meteorological-data-,with-developed-for the meteorological data: 0 being-measured-data-,indicates measured data; 1being-interpolated-data-, interpolated data; 2being data filled using the-a nearby station as a reference-,and-2-being-data-filled-with-ERA5-; 3, data filled using ERA5-Land as a reference.

Gaps in the flux time series were filled using a double-step procedure, analogous to the approach applied in ?Winck et al. (2023). Short gaps were filled using the Marginal Distribution Sampling method (?) (Reichstein et al., 2005) with the online version of the REdDyProc package (?) (Wutzler et al., 2018). Short gaps were considered by taking the filled data with quality flags of 0 (originally-original measured data) or 1 (highly-reliable-highly reliable filled data). Subsequently, the remaining gaps (flagged with 2 or 3 in REdDyProc) were filled using a machine learning (ML) tool based on the Extreme-Gradient-Boosting (XGBoost)

algorithm (Chen and Guestrin, 2016). The code was adapted from Vekuri et al. (2023) to include  $H$ ,  $LE$  and  $FC$ . The predictor variables of the model were the previously filled  $TA$ ,  $VPD$ ,  $SW\_IN$ ,  $WS$  and  $WD$ . The inclusion of  $WD$  followed the recommendation of Richardson et al. (2006) to account for the heterogeneity of the site, with site heterogeneity, as different land covers depending on wind sectors potentially contributing can contribute to flux variability. A quality flag was developed for flux variables, being developed for the flux variables: 0 for measured data, 1 for data filled with REdDyProc, and 2 for data filled with XGBoost. There were two very long gaps, one for AF3 during summer 2023 (mid-July until beginning of October) and another for AF1 during winter 2023/24 (beginning of December 2023 until beginning of March 2024), besides gaps of few days duration. Such long gaps would introduce significant uncertainty into any gap-filling method, the analysis considered only measured data so the analysis only considered measured and gap-filled data for gaps not exceeding two weeks duration.

The error in evaluation of the gap-filled fluxes with XGBoost was taken as the performed by splitting the initial dataset into 80 % training data and 20 % test data. The root mean squared error (RMSE) of the modelled data. Table 1 shows the RMSE scores for  $FC$ ,  $LE$  and  $H$  for all four stations. RMSE between modeled and measured data, for the test dataset, was taken as the error attributed to each individual gap-filled in the individual 30-minute flux value (Table 1).

**Table 1.** Root mean squared error (RMSE) of modeled and measured data, for  $FC$ ,  $LE$  and  $H$ , for the four stations used in this study. Note that the error in  $FC$  was slightly different across the stations, but the displayed values are similar due to the effect of decimal rounding.

	AF1	AF2	AF3	MC-OC
$FC$ ( $\mu\text{mol m}^{-2}\text{s}^{-1}$ )	2.8-3.1	2.8-3.2	2.8-3.4	2.8-3.2
$LE$ ( $\text{W m}^{-2}$ )	23.2-24.2	32.8-25.0	19.7-20.2	25.7-26.5
$H$ ( $\text{W m}^{-2}$ )	14.5-14.7	15.2-13.5	13.0-13.2	14.1-14.4

### 2.3.4 Footprint calculation.

A footprint climatology was calculated for all stations, for five different periods considered in the study: (i) growing season 2023: from March to 13 July 2023, with the latter being the harvest date of rapeseed; (ii) harvest period 2023: from 13 July to 22 September 2023, with the latter being the harvest date of corn; (iii) winter 2023/24: from 22 September 2023 to 1 March 2024; (iv) growing season 2024, from 1 March to 15 July 2024, with the latter being the harvest date of the rapeseed; and (v) harvest period 2024, from 15 July to 19 September 2024. The footprint climatology was calculated using the Python version of the model by Kljun et al. (2015).

The input data for the footprint model comprised included non gap-filled wind data ( $WS$ ,  $\text{m s}^{-1}$ , and  $WD$ ,  $^\circ$ ), roughness length ( $z_0$ , m),  $USTAR$ , Obukhov length ( $L$ , m), the standard deviation of lateral wind speed ( $V\_SIGMA$ ,  $\text{m s}^{-1}$ ), boundary layer height ( $BLH$ , obtained from ERA5, Hersbach et al. 2023), measurement height ( $z_m$ , m), and displacement height ( $d_h$ , m). Daytime and nighttime values were used for the footprint modeling.  $z_0$  and  $d_h$  were estimated from the aerodynamic canopy height ( $h_a$ , m). Only daytime values were selected based on values of  $SW\_IN$  higher than  $10 \text{ W m}^{-2}$ . The aerodynamic



canopy height was calculated during  $\overline{ZL(z-d)/L} \leq 0.1$  based on the procedure by  $\overline{?}$ . The complete time series of  $h_a$  were estimated as by calculating the running mean of  $h_a$  for eight different wind sectors of  $45^\circ$  each, using a running mean of 100 30-min intervals. This procedure is described in more detail in van Ramshorst et al. (in prep.). This procedure allowed for a more comprehensive representation of the roughness-effects of a varying canopy, therefore it can be considered as a more precise representation compared to the use of roughness and is therefore more precise than using a single value representing to represent the average canopy height for the whole site for entire site at each time step.  $d_h$  and  $z_0$  were estimated-calculated as 0.6 and 0.1 times the aerodynamic canopy height, following  $\overline{?}$  respectively, following Chu et al. (2018). The mean values of  $d_h$  were 3.1 m at the AF and 0.6 m at the MCOC, while the mean values of  $z_0$  were 0.5 at the AF and 0.1 m at the MCOC. A thorough discussion on the uncertainties of the footprint model about the footprint model uncertainties can be found in Section 4.4.

## 2.4 Spatial and temporal variability of fluxes and turbulence parameters and effect size

In order to To disentangle spatial and temporal variability of fluxes and turbulence parameters across the site, the data were classified in two different ways. Firstly, ways. First, the data were aggregated according to different into wind sectors of  $3045^\circ$  each, similar to the sectors used for the planar fit division (see section 2.3), and separated into five time periods as described in the previous paragraph. Secondly, Second, the data were grouped in periods of one week, along the whole measurement campaign, without the into one-week periods throughout the entire measurement campaign without division into wind sectors. For each of these classifications classification, coefficients of spatial variation (CVs) were calculated and the variance was partitioned into temporal and spatial components. In this analysis used only measured data filtered according to the previously described criteria, not gap-filled data.

The CVs were defined as follows

$$CV_x = \left[ \frac{\overline{< [x(t) - X(t)]^2 >^{\frac{1}{2}}}}{X(t)} \right] \quad (1)$$

based on  $\overline{?}$  and  $\overline{?}$  Katul et al. (1999) and Oren et al. (2006).  $X$  is the spatial average of variable  $x$  across the three towers in the AF for the respective averaging time interval. Angular brackets ( $<>$ ) denote the spatial averaging operator and the overbar denotes temporal average across all the individual time steps  $t$ . This formula was applied to  $H$ ,  $LE$  and  $FC$ , and to the standard deviation of the vertical wind velocity ( $W\_SIGMA$ ,  $\text{m s}^{-1}$ ),  $USTAR$  and  $WS$ . The coefficients of variation are dimensionless, normalized by the spatial average of variable  $x$ , such that they can be compared for between different variables. Lower limits were set for some of the variables, in order to avoid biasing the coefficients of variation by some very low fluxes in the denominator of Equation 1. These limits were  $10 \text{ W m}^{-2}$  for  $H$  and  $LE$ ,  $\pm 2 \mu\text{mol m}^{-2} \text{ s}^{-1}$  for  $FC$ , and  $0.5 \text{ m s}^{-1}$  for  $UWS$ .

The partitioning of the variance into temporal and spatial components was done as presented in  $\overline{?}$  Peltola et al. (2015) (Eq. 2 therein) based on  $\overline{?}$  Sun et al. (2010):

$$\sigma_{tot}^2 = \frac{m(n-1)}{m \cdot n - 1} \sigma_s^2 + \frac{n(m-1)}{m \cdot n - 1} \sigma_t^2(\xi) = \sigma_s + \sigma_t \quad (2)$$



with  $m$  the number of temporal data points,  $n$  the number of measurement locations,  $\bar{\sigma}_s^2$  the time average of the spatial variance, and  $\sigma_t^2(\xi)$  is the temporal variance of the time series of spatial averages  $\xi$ . Consequently, the first term on the right hand side of the equation is equivalent to the spatial variance ( $\sigma_s$ ), which includes as well the instrumental variance, while the second term is equivalent to the temporal variance ( $\sigma_t$ ) (Peltola et al., 2015).

Furthermore, the effect size ( $d$ ) was calculated in order to assess the statistical robustness of our distributed network, in accordance with the hypothesis of Hill et al. (2017) that the enhanced error observed in LC-EC setups can be counteracted by an improved statistical representativeness of the measurements, provided that the effect size is sufficiently large. In our case, with the ~~three-towers~~ three-tower network we calculated  $d$  across the three towers inside the AF and between the AF and the ~~MEOC~~.  $d$  was calculated, following ~~?~~, as Hill et al. (2017), as

$$d = \left| \frac{f_1 - f_2}{\sigma} \right| \quad (3)$$

where  $f_1$  is the flux from ecosystem 1,  $f_2$  is the flux from ecosystem 2 and  $\sigma$  is the pooled standard deviation of data from both ecosystems.  ~~$d$  can be positive or negative.~~ We used daily cumulative sums of gap-filled  $FC$  and  $LE$ . The value  $f_1$  in Eq. 3 refers to the daily cumulative sums of  ~~$FC$~~  (g C m<sup>-2</sup>) or  $LE$  (W m<sup>-2</sup>) at the AF, as an average across the three stations, while  $f_2$  corresponds to the daily cumulative sum of  ~~$FC$~~  or  $LE$  for AF1 or for ~~MEOC~~, depending on the case under study. We calculated  $d$  for two different cases: (i) to test whether fluxes over AF (~~average-averaged~~ across the three towers) ~~were significantly different~~ differed significantly from fluxes over ~~MC, in order-OC~~, to compare both ecosystems; and (ii) to test whether fluxes over AF ~~were significantly different from fluxes from~~ differed significantly from those of the reference tower AF1, in order to compare the increase in statistical robustness of the distributed network to the hypothetical case in which only one station was installed at the AF. AF1 was selected as the reference tower because it was the ~~oldest-running~~ longest-running tower on site, having been in operation since 2016.  $\sigma$  was calculated as in ~~?~~ Hill et al. (2017)

$$\sigma = \sqrt{\frac{(n_1 - 1)\sigma_1^2 + (n_2 - 1)\sigma_2^2}{n_1 + n_2 - 2}} \quad (4)$$

where  $\sigma_1$  and  $\sigma_2$  are the standard deviations of both datasets being compared, and  $n_1$  and  $n_2$  are the number of data points in each of the datasets.  ~~$\sigma$  was  $\sigma_1$  and  $\sigma_2$  were~~ calculated as the error of the daily cumulative ~~sums~~ sums, from the individual 30-min error in the fluxes (see next section). Afterwards Eq. 4 was applied to get the error for the ensemble of stations being compared.

## 2.5 Uncertainty of the LC-EC setups

The uncertainty in  $FC$  and  $LE$  was considered by assigning an error to each 30-min flux value. This error was ~~propagated later on-then propagated~~ when aggregating data to daily cumulative sums for the effect size calculations. The error was considered differently for measured and gap-filled data. ~~In the case of~~ For measured data, the error in the 30-min  $FC$  and  $LE$  was obtained from the inter-comparison of LC-EC and conventional EC setups in the studies of ~~?~~ and ? ~~Callejas-Rodelas et al. (2024) and van Ramshorst et al. (2024)~~. The error was taken as the worst-case ~~slope of the linear regression models RMSE of all the comparisons~~ between LC-EC and conventional EC setups, separately for  $FC$  and  $LE$ . ~~It was of 5% The values were 3.1  $\mu$ mol~~

322  $\text{m}^{-2} \text{s}^{-1}$  and  $44.1 \text{ W m}^{-2}$ , respectively, for *FC* and ~~22% for *LE*~~. This error was considered as a relative error for each  
 323 individual flux value. It is important to note that the error is a systematic deviation from the conventional EC setup, and no  
 324 random error was considered in these calculations. Therefore, the uncertainty associated with a given flux value is determined  
 325 by the product of this error value and the magnitude of the flux itself. As an example, a *FC* of  $10 \text{ mol m}^{-2} \text{s}^{-1}$  would be  
 326 expressed as  $10 \pm 0.5 \text{ mol m}^{-2} \text{s}^{-1}$ , and a *LE* of  $100 \text{ W m}^{-2}$  would be expressed as  $100 \pm 22 \text{ W m}^{-2}$  not a random error.

327 In the case of the ~~For~~ gap-filled data, the error was addressed differently for the two gap-filling steps. For the data filled  
 328 with REddyProc, the error was defined as the standard deviation of the data points used for gap-filling (?) (Wutzler et al., 2018)  
 329 , provided as an output from the REddyProc processing. In contrast, for the data filled with XGBoost, the individual error in  
 330 the fluxes was assigned as the RMSE of the modelled data (Table 1). The uncertainty in a cumulative sum was then calculated  
 331 using error propagation from the single 30-minute uncertainties to the daily sums.

## 322 3 Results

### 333 3.1 Meteorological conditions

334 *SW\_IN* followed a seasonal cycle, ~~with the maximum magnitude~~. The maximum magnitude was observed at the end of June  
 335 2023(, with daily means above  $300 \text{ W m}^{-2}$ ), followed by a radiation intensity decrease, reaching the minimum values in winter  
 336 decrease in radiation intensity. Minimum values close to  $0 \text{ W m}^{-2}$  were reached in winter, and then again increasing until the  
 337 intensity increased again until reaching similar maximum values in June 2024 (Fig. 2a). Monthly Total monthly values of *P*  
 338 were large, especially from June to December in 2023, and in July of 2024, with values reaching up to 125 mm (Fig. 2d).  
 339 There were some very dry months, with *P* sums lower than 20 mm, especially from March to June in 2024. Compared to  
 340 the climatological averages (Table 2), all seasons during the measurement period were more rainy than the period 1981-2010,  
 341 especially during summer and autumn of 2023, when the recorded precipitation was more than three times the reference one  
 342 value (272 mm vs. a reference value of 65 mm for summer 2023, and 218 mm vs. a reference value of 52 mm for autumn 2023).  
 343 Only spring Spring 2024 was slightly dryer the only season slightly drier than the climatological reference, with a record of 30  
 344 mm of rain instead of 49 mm.

345 *TA* followed a seasonal cycle, with the lowest values in winter (daily means between 0 and  $10^\circ\text{C}$ , with occasional lower  
 346 values) and the highest values in July and August of both 2023 and 2024 (daily means around  $20^\circ\text{C}$ ). *TA* was slightly larger  
 347 at the MC-OC tower than at the other three AF towers during most of the campaign, with enhanced differences in summer  
 348 and very small differences in winter. The mean *TA* during the campaign was  $12.86^\circ\text{C}$  at the MCOC, while it was  $12.49^\circ\text{C}$  at  
 349 the AF. The three AF stations showed very similar *TA*. *TA* was higher in all seasons compared to the climatological averages  
 350 (Table 2), except in spring 2023 in which both values were similar ( $9.1^\circ\text{C}$ ). Summer 2023 and summer 2024 were slightly  
 351 warmer ( $18.7$  and  $18.64^\circ\text{C}$ , respectively) than the reference value ( $17.4^\circ\text{C}$ ). Autumn 2023, winter 2023/24 and spring 2024  
 352 were clearly warmer than the climatological averages, with  $11.9$ ,  $4.3$  and  $11.8^\circ\text{C}$  vs. the reference values of  $9.8$ ,  $1.7$  and  $9.1$   
 353  $^\circ\text{C}$ , respectively. The absolute difference between measured and historical data was largest in winter.

**Table 2.** Measured and reference climatological averages of *TA* and *P* by seasons. Measured seasonal values were calculated as averages across all four stations at the site. Reference values were taken as the seasonal 1981-2010 climatological average from the German Weather Service ([https://opendata.dwd.de/climate\\_environment/CDC/observations\\_germany/climate/](https://opendata.dwd.de/climate_environment/CDC/observations_germany/climate/), last accessed 25-09-2024) from the nearby station at Braunschweig airport (ID 662).

Season	Measured <i>TA</i> (°C)	Measured <i>P</i> (mm)	<i>TA</i> reference (°C)	<i>P</i> reference (mm)
Spring 2023	9.1	102.5	9.1	48.7
Summer 2023	18.7	272.3	17.4	65.0
Autumn 2023	11.9	218.5	9.8	52.0
Winter 2023/24	4.3	198.0	1.7	46.7
Spring 2024	11.8	30.1	9.1	48.7
Summer 2024	18.6	165.8	17.4	65.0

*VPD* values also showed a marked seasonality (Fig. 2c). Values were very low in winter, between 0 and 0.2 kPa, and increased towards summer in both 2023 and 2024, reaching daily means between 1 and 1.5 kPa. ~~*VPD* was still relatively large~~, while in autumn of 2023 ~~*VPD* was lower~~ with values of around 0.5 kPa. Comparing the four stations, the ~~MC-OC~~ site experienced a larger *VPD* from July to October 2023, while during the rest of the campaign no significant differences were observed across the stations. The mean *VPD* was 0.41 kPa at the ~~MC-OC~~ and 0.4 kPa at the AF as an average of the three stations. The differences between the three AF stations were very small.

### 3.2 Footprint climatology

~~The seasonal footprint climatology show the 80 % contributions from the different land uses to the fluxes by all four stations (Fig. 3).~~ All footprints exhibited larger contributions from the western side of the towers in all periods (growing season 2023, harvest period 2023, winter 2023/24, growing season 2024 and harvest period 2024), corresponding to the dominant wind direction at the site ~~(Fig. 3)~~. For all periods under consideration and for both 50 and 80 % footprint areas, the footprint of the ~~MC-OC~~ tower was smaller than for the three AF towers, due to the lower measurement height. At the AF, footprints decreased from 2023 (Fig. 3a and b) to 2024 (Fig. 3d and e), likely due to the increase in canopy height of the trees. In the case of the OC, footprints were similar during the growing season of 2023 compared to the growing season of 2024 (Fig. 3a and d), and smaller during the harvest period of 2023 compared to the harvest period of 2024 (Fig. 3b and e). The 50 % footprint climatology contribution was concentrated in a small area around the stations, covering only the two crop fields at both sides of the stations, plus one or two tree rows in the case of the AF. There were small variations from season to season and a partial overlap between towers AF1 and AF2, and towers AF2 and AF3.

The 80 % footprint climatology contribution was larger, covering a larger portion of both AF and OC sites and therefore a surface with a larger heterogeneity due to the presence of more diverse crops and/or trees. The three stations at the AF exhibited partially overlapping footprints for the 80 % footprint climatology, with different sizes and degrees of similarity depending on the evaluated period. The most intense overlap occurred during the growing season of 2023 (Fig. 3a). The 80 % footprint

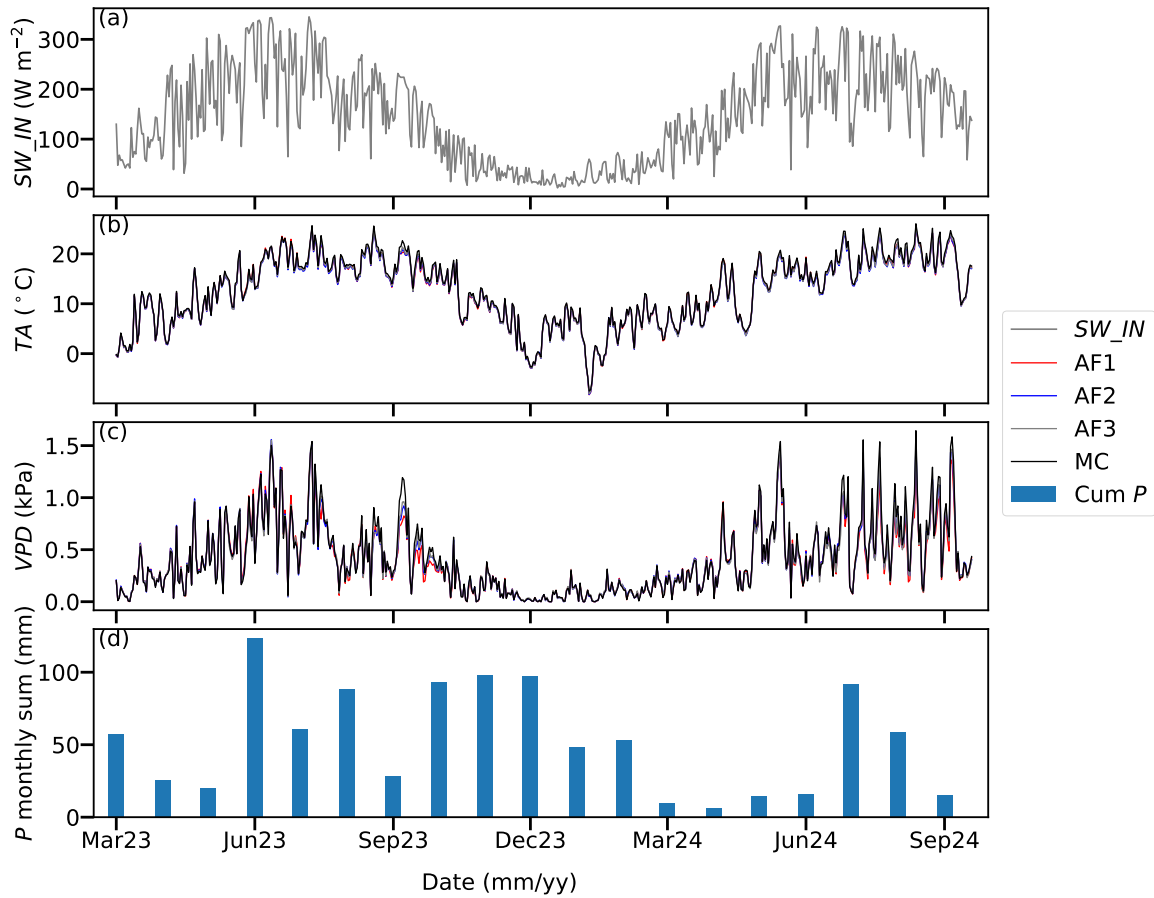


**Figure 2.** Time series of daily mean meteorological parameter and the cumulative sum of precipitation across the measurement campaign: (a) global radiation ( $SW\_IN$ ), (b) air temperature ( $VPD$ ), (c) vapor pressure deficit ( $VPD$ ) and (d) monthly sums of precipitation ( $P$ ).  $SW\_IN$  and  $P$  were considered as common to all the stations, because the size of the site is small enough to assume homogeneity in these parameters, whereas  $TA$  and  $VPD$  were plotted separately for all four stations. Data were filtered for outliers using lower and upper limits, gap-filled as detailed in Section 2.3.3, and then aggregated to daily values by taking the daily mean for  $SW\_IN$ ,  $TA$  and  $VPD$  and the daily sum for  $P$ .

of the three towers covered approximately four tree rows and four crop rows each. The three towers at the AF presented different footprint sizes, with the largest areas being covered by AF3, followed by AF2 and finally by AF1. The order of this rank of magnitude was the same in all seasons. The footprint from the MC tower covered both the western and eastern fields around the tower, but the contribution was larger from the western part in all seasons. For all stations, there were some contributions to the 80 % footprints from the areas beyond the AF or the MC fields. This was especially remarkable in the case of AF3, which had some contributions from the western side of the field in winter 2023/24 (Fig. 3e) and from the northern side of the field in both harvest periods of 2023 and 2024 and the 2024 growing season (Fig. 3b,d,e). However, the contributions of the areas outside the AF were expected to be negligible regarding the interpretation of the results.



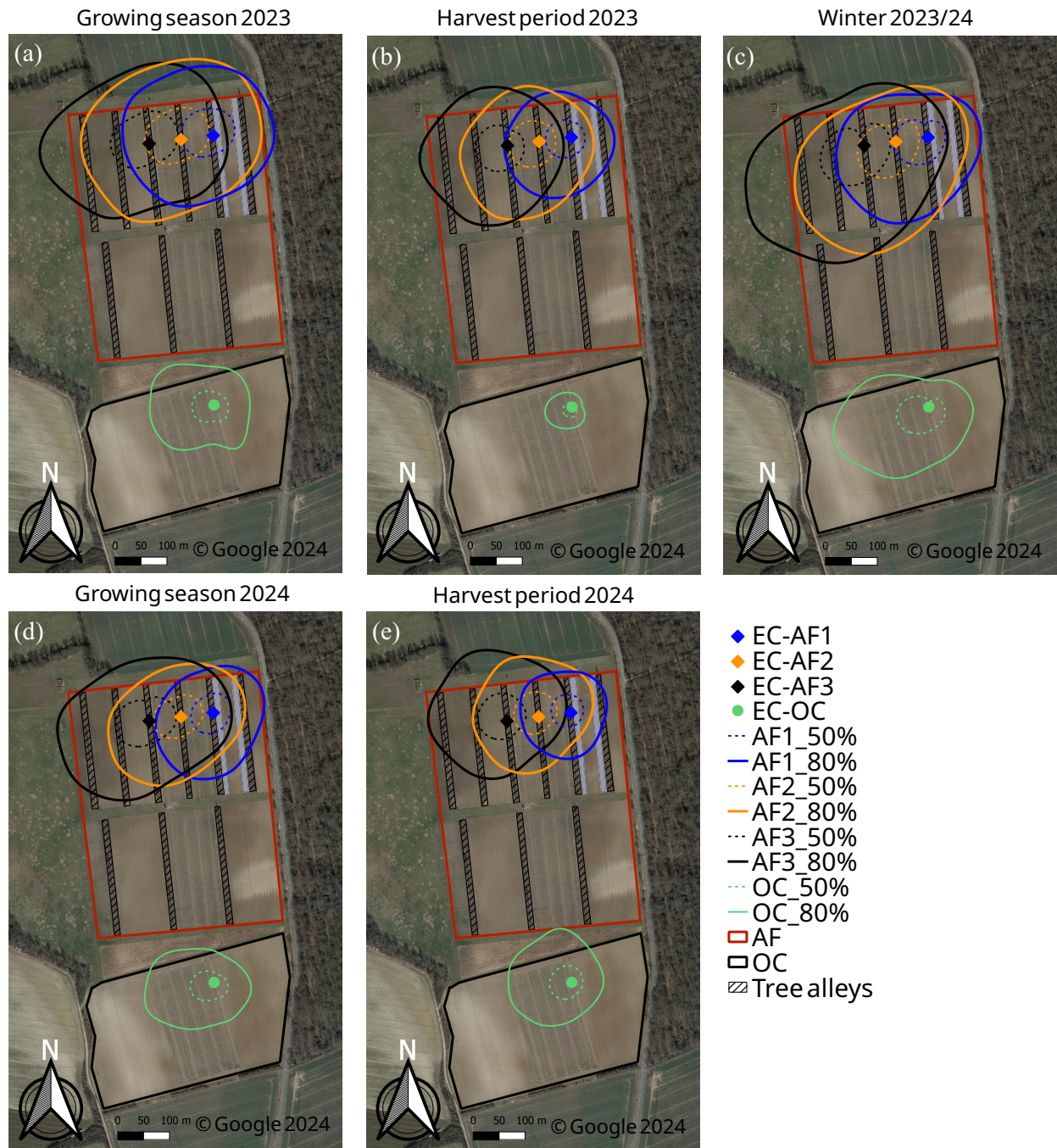


**Figure 3.** Footprint climatologies, calculated from the model of Kljun et al. (2015) as detailed in section 2.3.4, for the three towers at the AF (AF1, blue; AF2, orange; AF3, black) and the tower at the OC (green), divided into five different periods: growing season 2023 (a), harvest period 2023 (b), winter period 2023/24 (c), growing season 2024 (d) and harvest period 2024 (e). The lines plotted in the map represent the 80 % (solid line) and 50 % (dashed line) contributing areas to the footprint. The station locations are marked with diamonds for the AF stations and a circle for the OC station. Figure created with QGIS v. 3.22, aerial map by Google Satellite Maps. © Google 2024.



385 The analysis of the differences in land cover measured by the different stations revealed ~~variations from season to season.~~  
 386 ~~In the 2023 growing season, the footprints~~ seasonal variations. Because all the AF stations covered some of the tree rows,  
 387 specifically 3 or 4 in the case of AF1 , and 4 to 6 in the case of AF2 and AF3~~were overlapping the most compared to the other~~  
 388 ~~seasons,~~ the description of the differences will focus on the different crops covered by the 80 % footprints. During the growing  
 389 season of 2023 (Fig. 3a). At AF1 predominantly four tree strips, corn, barley and the nettle fiber rows were detected. At AF2,  
 390 the footprint encompassed a larger area, covering five tree strips, all three crops (rapeseed, corn and barley) plus the nettle fiber  
 391 ~~was detected.~~ At ~~the three stations at the AF covered all crops, whereby~~ AF3 only covered a small portion of the barley field  
 392 and the footprint was the most extensive, covering also five tree strips, the three crops and one of the nettle fiber strips, plus  
 393 some areas beyond the AF site was detected. The overlap of the footprints was more intense between towers AF2 and AF3.  
 394 ~~The MC tower detected mostly the corn field, with a small contribution of the rapeseed field.~~  
 395 During the harvest period in 2023 , the footprint size diminished, partially due to a reduced considered period. The footprint  
 396 climatology is a weighted average, hence, a longer evaluated period is likely to extend the footprint area. This led to a reduction  
 397 in the degree of overlap among the footprints, particularly between (Fig. 3b), AF2 covered all crops, including harvested  
 398 rapeseed, while AF1 and AF3. AF1 covered three tree strips, covered corn, barley (harvested at the end of August 2023) and  
 399 nettle fiber; AF2 covered four tree strips, only one row of rapeseed, the whole corn field and a small part of the barley field; and  
 400 AF3 covered also four tree strips, the whole rapeseed field and part of the corn field. The MC tower covered only part of the corn  
 401 field. Footprint climatologies, calculated from the model of ?, for the three towers at the AF and the tower at the MC (detailed  
 402 in Section 2.3.4), divided into five different periods: growing season 2023 (a), harvest period 2023 (b), winter period 2023/24  
 403 (c), growing season 2024 (d) and harvest period 2024 (e). The lines plotted in the map represent the 80 % contributing areas  
 404 to the footprint. Figure created with QGIS v. 3.22, aerial map by Google Satellite Maps. © Google 2024. rapeseed (harvested)  
 405 and corn. In winter 2023/24 (Fig. 3c), the footprint size increased again for all stations, enhancing the overlap. However, this  
 406 enhancement was not as substantial as the one observed during the 2023 growing season. All crops had been harvested, and  
 407 only the rapeseed had been sown in the eastern part of the field in September 2023 (Fig. 1b), therefore the remarkable features  
 408 of this season are that the footprints of both AF1 and AF2 covered one of the rapeseed field rows, together with the nettle fiber,  
 409 while the footprint of AF3 did not. The other spaces in between tree strips were bare soil during this season. The MC footprint  
 410 was larger than during the other seasons and covered most of the field in the west of the tower and a small part of the rapeseed  
 411 field in the east.  
 412 During the 2024 growing season, the footprints of AF1 and AF2 exhibited an overlap of approximately 50 % of the footprint  
 413 area, while the overlap between AF1 and AF3 was significantly less all towers covered most of the crop fields, but these were  
 414 mostly bare soil at this stage. During the growing season of 2024 (Fig. 3d) ~~- e~~, AF1 covered rapeseed, nettle fiber, part of the  
 415 barley field and only three tree strips rapeseed and barley; AF2 covered part of the corn field and the barley field, plus four tree  
 416 strips all crops; AF3 covered the whole corn and barley fields and five tree strips. The MC footprint reduced in size compare to  
 417 the winter period, and was mostly covering the barley field in the west of the station corn, barley and only a small portion of  
 418 rapeseed and nettle fiber. Finally, during the 2024 harvest period, the footprint size reduced again for all stations, and so did the  
 419 overlap (Fig. 3e). harvest period of 2024, AF1 covered only part of the barley field and part of the rapeseed field, together with

the nettle fiber and two tree strip nettle fiber, rapeseed (already harvested) and barley (harvested three weeks after the beginning of this period); AF2 covered most of the barley field and parts of the rapeseed and the corn fields, plus three tree strips; and all crops; AF3 covered the corn field, part of the barley field and almost four tree strips. The footprint of the MC was similar to the 2024 growing season (Fig. 3e) covering mostly the barley field corn and a minor portion of the rapeseed field barley. In all seasons, the OC tower covered mostly the western field (corn in 2023 and barley in 2024) and partially the eastern field (barley in 2023 and rapeseed in 2024).

### 3.3 Weekly sums of carbon and evapotranspiration

The weekly cumulative sums of  $FC$  (Fig. 4a4a) exhibited a marked seasonal behavior and similar variability across the four towers. The seasonal cycle was characterized by the uptake of carbon carbon uptake (negative values) during the growing season and carbon losses loss (positive values) during winter. The differences were smaller across the three AF towers, with AF1 and AF2 behaving more similar exhibiting more similar behavior. During the 2023 growing season, there was a strong uptake at all stations of around  $-30/-40 \text{ g C m}^{-2}$  per week at all stations, from April to September 2023. This was interrupted by the short dry period of three weeks which occurred a short, three-week dry period at the end of May and first half the beginning of June of 2023 (?) with (DWD, 2024), during which the AF site turning to a turned into a weak carbon source (as measured by AF2) or to a weak carbon sink (as measured by AF1 and AF3). The uptake was stronger at AF3 until mid June, after which MC showed stronger uptake until mid-June. After that, OC showed the strongest uptake ( $-40$  to  $-60 \text{ g C m}^{-2}$  per week) for the rest of the growing season. After the harvest of the rapeseed rapeseed harvest on 13 July 2023, weekly sums reduced the weekly sums decreased in magnitude but were still large remained substantial at AF1, AF2 and MC-OC (AF3 was missing during this period), and after the harvest of the barley. Around the barley harvest on 22 August 2023 the sums reduced decreased notably. From October 2023 to March 2024, the values were positive and comparable across all stations, indicating a carbon release from the ecosystems. During the 2024 growing season, the carbon uptake was found to be carbon uptake diminished compared to the 2023 growing season. The strongest uptake of around  $-25 \text{ g C m}^{-2}$  per week occurred in July 2024. AF2 and MC-OC showed the strongest uptake during in June and July, however, after the harvest of the rapeseed. However, after the rapeseed harvest on 15 July, the uptake reduced decreased, and AF2 and MC changed their sign towards OC changed to a carbon source, while. Meanwhile, AF1 and AF3 still showed negative values. After the harvest of the barley barley harvest on 5 August 2024, the uptake of at AF1 and AF3 reduced even more, changing in decreased further, with AF1 towards changing to a carbon source. AF3 kept exhibited a  $\text{CO}_2$  sequestration behavior until the end of the measurement period.

The weekly cumulative sums of  $ET$  (Fig. 4b) also exhibited a strong seasonality in all stations and similar variability across them all stations. During the 2023 growing season, there were increasing  $ET$  weekly sums the weekly  $ET$  sums increased from April (values around  $10 \text{ mm}$  per week) until the maximum values attained were reached in July, with a magnitude of  $30 \text{ mm}$  at AF2, AF3 and MCOC, and  $40 \text{ mm}$  at AF1. Afterwards there was a progressive reduction in  $ET$ , especially enhanced after the harvest of the rapeseed rapeseed harvest on 13 July 2023 and the harvest of the corn corn harvest on 26 September 2023. AF1 showed the highest values until October 2023. Thereafter After that, all stations showed low values coinciding with the winter period, of around  $5 \text{ mm}$  per week, coinciding with the winter period, until March 2024. During the 2024 growing season,

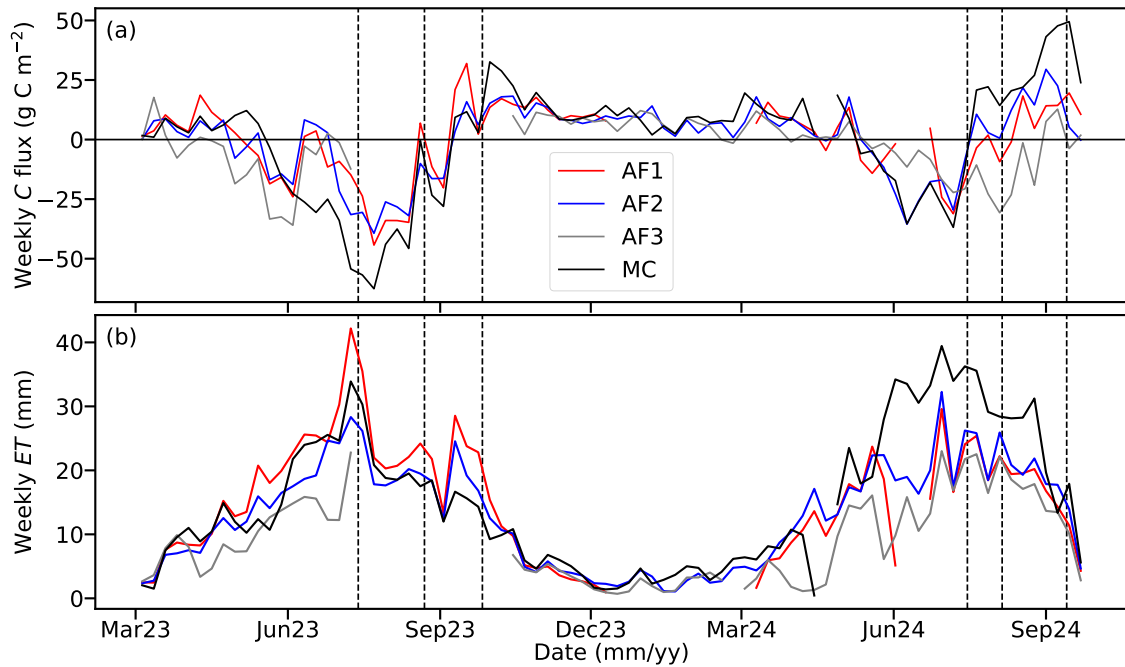


**Figure 4.** Weekly sums of the net ecosystem carbon exchange as a carbon (C) flux (a) and evapotranspiration (b, *ET*) measured at the four stations, across the measurement campaign. Sums were calculated from the gap-filled time series. Missing values correspond to gaps longer than 2 weeks, which were not considered in the analysis. The horizontal line in sub-plot (a) highlights the zero line, separating the uptake (negative fluxes) from the emission (positive fluxes). Vertical dashed lines represent, from left to right, the harvest dates of rapeseed (13 July 2023), barley (22 August 2023) and corn (26 September 2023) in 2023; and rapeseed (15 July 2024), barley (5 August 2024) and corn (13 September 2024). Due to the requirement of taking only gap-filled data for gaps up to two weeks of duration, there were some missing weeks for all stations and two very long gaps, in summer 2023 for AF3 and in winter 2023/24 for AF1.

454 ~~weekly-ET was again progressively increasing-increased~~ progressively at all the stations ~~,-until they reached-until reaching~~ the  
 455 maximum values of 30 and 40 mm. ~~The-increase-was-only-interrupted-This increase was interrupted only~~ by a reduction in  
 456 *ET* in June, more ~~marked-pronounced~~ at the AF towers. After the peak of the growing season, *ET* reduced especially after  
 457 the ~~harvest-of-the-rapeseed-rapeseed harvest~~ on 15 July 2024 and the barley on 5 August 2024. The highest values during  
 458 the ~~growing-season-2024 growing season and harvest period~~ were found for the ~~MC-until July-and-for-AF2-after-that,-and~~  
 459 ~~the-reduction-in-ET after the harvest events-was more marked-in these two stations-AF1-and-OC.~~ AF3 kept lower values and  
 460 ~~exhibited-a-more-similar-behavior~~ exhibited lower values at the beginning of the growing season, but the three towers at the AF  
 461 showed a good agreement from July on.

## 3.4 Coefficients of variation, spatial and temporal variance

### 3.4.1 Classification in wind direction bins

The CVs calculated at the half-hourly scale (Eq. 1) were the largest for  $FC$  in most of the wind sectors and the eastern and southeastern wind sectors ( $60-180^\circ$ ) and all the evaluated periods, followed by the CVs of  $LE$  and  $H$  (Fig. 5). The CVs of  $WS$ ,  $USTAR$  and  $W\_SIGMA$  were low in comparison to largest values of the CVs of  $FC$ ,  $LE$  and  $H$ . The lowest variability across wind sectors in all periods was found for  $W\_SIGMA$ , followed by  $USTAR$  and  $WS$ , with CV values below 0.15 in most of the cases. Within the were reached during the 2023 growing season,  $FC$  showed the largest spatial variability in the eastern and southern wind sectors, with up to 8.4. The magnitude of the CVs above 0.5 and up to 1.2.  $LE$  and  $H$  showed similar values of between 0.2 and 0.3, slightly higher for  $LE$  (close to 0.4) in the northern wind sectors ( $330-60^\circ$ ). During the 2023 harvest period, no CVs of  $FC$  and  $LE$  could be calculated due to the absence of data from AF3, therefore only the variability of was comparable to the magnitude of the CVs of  $HLE$  and turbulence parameters could be addressed.  $H$  showed the largest variability in the northeastern wind sectors ( $0-150^\circ$ ) in the other wind sectors and periods, with values of CVs of above 0.2. In winter 2023/24 between 0.25 and 0.4. Notably, the CVs of  $FC$  were larger during the harvest period of 2024 than during the largest in the eastern half ( $0-180^\circ$ ), with values between 0.2 and 0.8, while  $LE$  and  $H$  showed similar values between them; in the sectors  $180-270^\circ$  the CVs of  $LE$  were the largest, with values up to 0.6, followed by CVs of  $FC$ . For the sectors  $270-360^\circ$  the CVs of all variables were smaller than 0.3 and very similar across them. During the 2024 growing season,  $FC$  showed the largest variability in the eastern ( $30-180^\circ$ ) and northeastern sectors ( $330-30^\circ$ ), with values between 0.4 and 1.7, while the. The CVs of  $LE$  were similar to the CVs of  $H$  with a magnitude between 0.2 and 0.4. In the western sector ( $180-330^\circ$ ), however, the CVs of  $LE$  were the largest, with values between 0.4 and 0.5, and  $WS$ ,  $USTAR$  and CVs of  $FC$  were similar.  $W\_SIGMA$  were low compared to the CVs of  $H$ . Finally, during the 2024 harvest period, in the eastern sector ( $0-180^\circ$ ) the CVs of  $FC$ ,  $LE$  and  $H$  were very similar, with values between 0.2 and 0.4, and in the western sector ( $180-360^\circ$ ) the CVs of  $LE$  were slightly larger, between 0.4 and 0.5, and CVs of  $FC$  and  $H$  remained similar. The lowest variability across wind sectors in all periods was found for  $W\_SIGMA$ , followed by  $USTAR$  and  $WS$ , with CV values below 0.15 in most of the cases.

Both for  $FC$  and  $LE$ , both variance values were larger during the growing season and the harvest period in both years than during winter, due to the larger magnitude of fluxes. As an overall picture,  $\sigma_s$  was larger than  $\sigma_t$  in the western and northeastern wind sectors. Due to the scope of this analysis, it is important to remark in which wind sectors  $\sigma_s$  was larger than  $\sigma_t$ . Looking first at  $LE$  (Fig. 5, mid row)  $\sigma_t$  dominated the variance in all wind sectors during the 2023 growing season. During winter 2023/24,  $\sigma_t$  of  $LE$  was larger than  $\sigma_s$  in all sectors except in the bin  $210-240^\circ$ , when  $\sigma_s$  was much was larger than  $\sigma_t$ . During the 2024 growing season,  $\sigma_s$  was larger than  $\sigma_t$  in the wind sectors of  $60-90^\circ$  only in the sectors  $225-270^\circ$  and  $300-330^\circ$   $15-360^\circ$ . Finally, during the harvest period in 2024, the spatial component was larger than the temporal one only in the sector  $60-90^\circ$  during the winter 2023/24. For all other wind sectors and periods,  $\sigma_s$  was lower than  $\sigma_t$ .

Regarding  $FC$  (Fig. 5, bottom row), the picture was different compared to  $LE$ , with a higher relevance of the spatial component of the variance. During the 2023 growing season  $\sigma_s$  was larger than  $\sigma_t$  dominated all wind sectors except for the bins  $60-90^\circ$  in the northeastern sector ( $0-45^\circ$  and  $150-180^\circ$ ) and the southern half ( $90-270^\circ$ ), but the values of  $\sigma_s$  were close to the

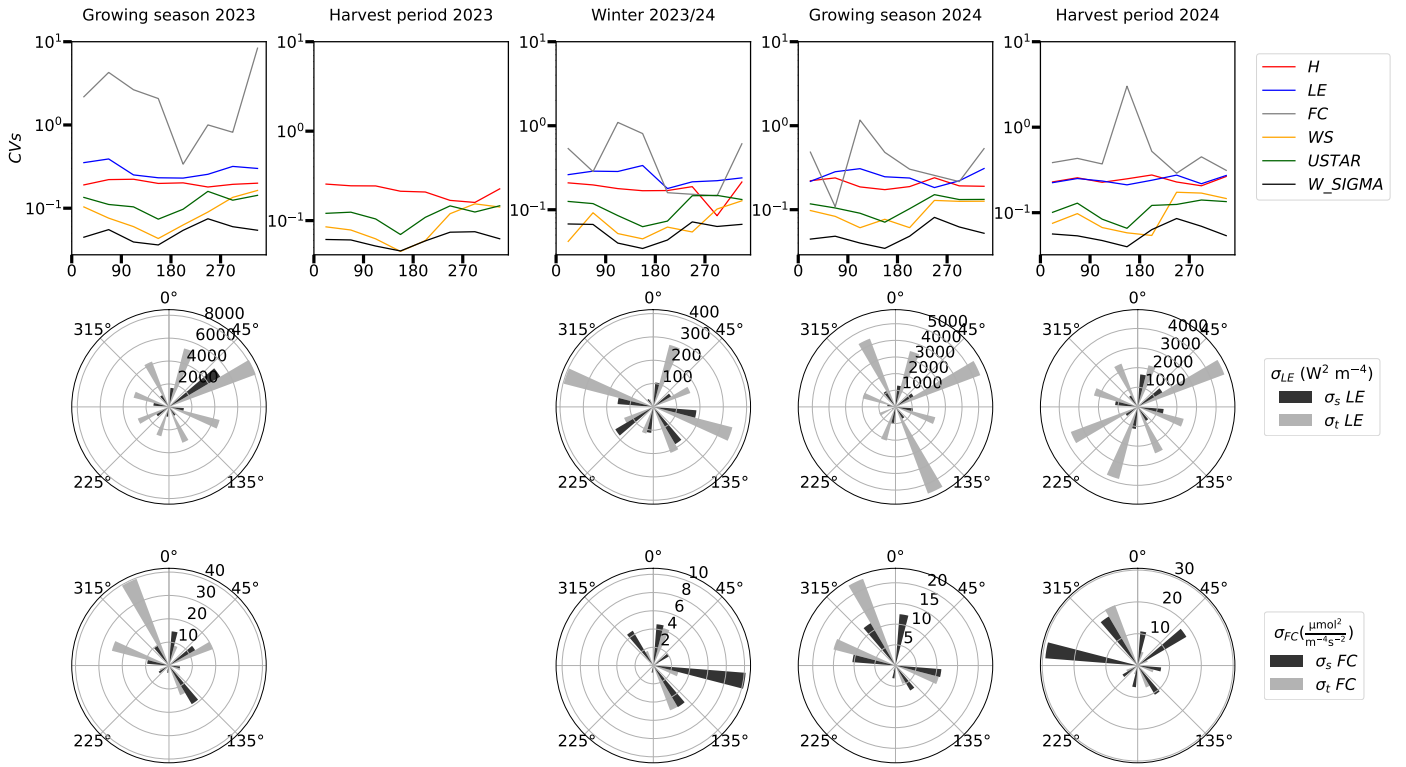


**Figure 5.** (Top row) Coefficients of variation (CVs), calculated after [Oren et al. \(2006\)](#), for *FC*, *LE* and *H*, *WS*, *USTAR*, and *W\_SIGMA*; (mid row) spatial ( $\sigma_s$  *LE*) and temporal ( $\sigma_t$  *LE*) variance for *LE*; (bottom row) spatial ( $\sigma_s$  *FC*) and temporal ( $\sigma_t$  *FC*) variance for *FC*. Data were grouped in all cases by wind direction bins of  $30^\circ$  each and separated into the five analysis periods (growing season 2023, harvest period 2023, winter 2023/24, growing season 2024 and harvest period 2024) detailed in Section 2.3.4. Due to the two very long gaps in AF1 and AF3 (see Fig. [??4](#)), plus some shorter gaps, there were no data corresponding to the harvest period in 2023 for *FC* or *LE*, therefore the sectorial plots for the variance partition are missing. Note that in the first row, due to the large magnitude of some of the CVs of *FC*, the variability in the lines corresponding to the other variables is more difficult to visualize. Note that the y-axis is in logarithmic scale in the CV plots, to facilitate visualization. Note also that the scale is different in the circular plots, depending on the magnitude of what is represented in each season. No gap-filled data were used to create this plot.

values of  $\sigma_t$  in all the eastern sectors). During winter 2023/24,  $\sigma_s$  was larger than  $\sigma_t$  in all wind sectors except  $0-30^\circ$ , with the largest difference in the eastern ( $90-120^\circ$ ) and southwestern ( $210-240^\circ$ ) sectors, and with relatively large values in the sectors  $120-210^\circ$ . During the 2024 growing season,  $\sigma_s$  was larger than  $\sigma_t$  in all sectors except in the northwestern ones ( $300-360^\circ$ ), the eastern and southern sectors ( $0-270^\circ$ ), reaching very large values in comparison to other periods (up to  $80 \text{ mol}^2 \text{ m}^{-4} \text{ s}^{-2}$ ) in the eastern half. Finally, during the 2024 harvest period,  $\sigma_s$  was larger than  $\sigma_t$  in the sectors  $0-60^\circ$  all sectors except in the Northwest ( $315-360^\circ$  and  $150-240^\circ$ , while  $\sigma_t$  dominated in the northwestern sectors).

### 502 3.4.2 Classification in weekly intervals

503 The weekly CVs across the measurement campaign were largest for *FC*, with a large difference to the ~~rest of the variables being~~  
504 ~~evaluated other evaluated variables~~ (Fig. 6a). The difference was especially remarkable during winter and from March to May  
505 ~~in both years 2023 and 2024. At the beginning of the 2023 growing season, in March and April~~ During most weeks, the CVs  
506 of *FC* ~~were between 0.3 and 2, much larger than the CVs of *LE*, while in May, June and until mid July (when the large gap in~~  
507 ~~*AF3* started), ranged between 0.2 and 4.0, but reached high values of around 30 in some specific times of the growing season~~  
508 ~~in both years and during winter. The CVs of *FC* and *LE* were similar, with values between 0.2 and 0.5, except for a very large~~  
509 ~~value of 10 the first week of June. In the short evaluated winter period, CVs of *FC* were very large in comparison to the other~~  
510 ~~variables, with values up to 3.9, and one very large value of 48. However this value could be classified as an outlier because of~~  
511 ~~the larger noise and uncertainty in the winter data. The much larger than the CVs of *LE* showed a small variability and were~~  
512 ~~close to and *H*, with values between 0.1 and 0.3. During the while in the summer months (after June) and the harvest period in~~  
513 ~~both 2023 and 2024 growing season, in March and April the the CVs of *FC* were large, with values up to 17 in March, while~~  
514 ~~CVs of *LE* were between 0.3 and 0.5, and CVs of *H* between 0.2 and 0.3. From May 2024 *LE* were similar, the CVs of *FC*~~  
515 ~~were similar to the CVs of *LE*, with values around 0.5 and slightly lower during the 2024 harvest period, and followed closely~~  
516 ~~between 0.2 and 0.5, closely followed by the CVs of *H*. During the whole Throughout the entire~~ campaign, the CVs of *USTAR*,  
517 and *W\_SIGMA* were much lower than for *H*, *LE* and ~~the~~ *FC*, similar as shown in Figure 5, with values below 0.2 across the  
518 ~~whole entire~~ period. However, the CVs of  $\bar{u}$ -*WS* were similar to ~~the ones those~~ of *H* during the growing season ~~as well as and~~  
519 the 2023 harvest period. After summer 2023 the CVs of  $\bar{u}$ -*WS* reduced their magnitude. The CVs of *USTAR*, and *W\_SIGMA*  
520 were the lowest and did not change much during the campaign. In general, ~~there was no clear effect of the harvest event on the~~  
521 ~~harvest events did not clearly affect the~~ variation of CVs for all variables.

522 With regards to partitioning the variance into its temporal and spatial components,  $\sigma_t$  was higher than  $\sigma_s$  for both *LE* and *FC*  
523 (Fig. 6b and 6c) during ~~all the evaluated periods. the summer months in both year. During winter and the months of March and~~  
524 ~~April, both variance components were of similar magnitude for *LE* and *FC*.~~ The highest variance (for both components) was  
525 observed during the end of the growing season in both years and during the harvest period in 2024, while the lowest occurred  
526 in winter time. ~~During winter,  $\sigma_s$  and  $\sigma_t$  were very similar for both *LE* and *FC*. The spatial variance of *LE* and *FC* was largest~~  
527 ~~in the summer months of both years. However, the difference between  $\sigma_t$  and  $\sigma_s$  changed from *LE* to *FC*. In the case of *LE*,~~  
528  ~~$\sigma_s$  was very close to  $\sigma_t$  from March to August 2024, being even higher in some weeks, and decreased largely in the harvest~~  
529 ~~period. In the case of *FC*,  $\sigma_s$  stayed at very low values in comparison to  $\sigma_t$  during the whole period. The The effect of harvest~~  
530 events in 2024 was shown by a ~~lower variance in both temporal and spatial components, especially visible in the case of *LE*~~  
531 ~~for which reduction in the difference between  $\sigma_t$  and  $\sigma_s$  reduced sharply after the harvest of the rapeseed in 2024 compared to~~  
532 ~~previous summer months and a reduction in the variance magnitude~~ (Fig. 6b).

### 533 3.5 Effect size and statistical representativeness of the three-towers network



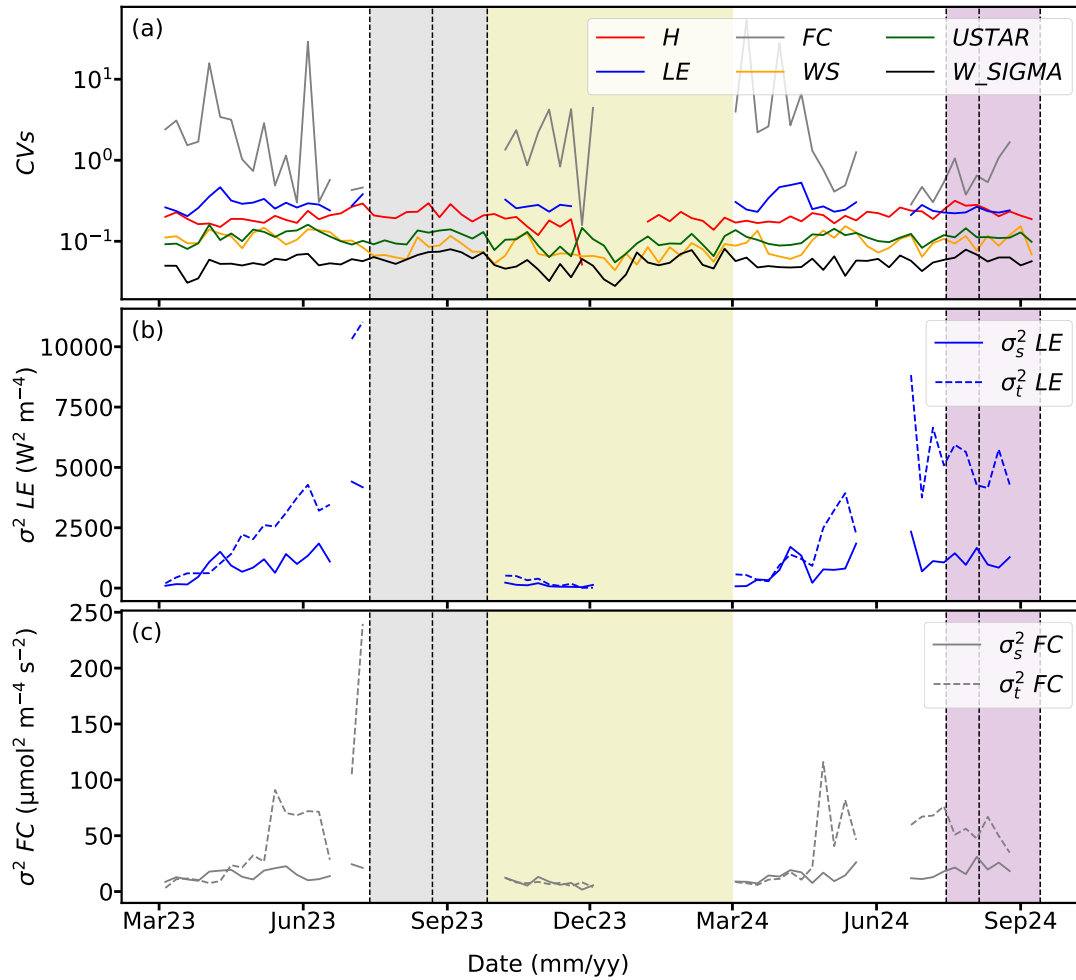


**Figure 6.** (a) Coefficients of variation (CVs), calculated after [Oren et al. \(2006\)](#), for  $FC$ ,  $LE$  and  $H$ ,  $\bar{u}$ ,  $USTAR$ , and  $W\_SIGMA$  (logarithmic scale); (b) spatial ( $\sigma_s^2 LE$ ) and temporal ( $\sigma_t^2 LE$ ) variance for  $LE$ ; (c) spatial ( $\sigma_s^2 FC$ ) and temporal ( $\sigma_t^2 FC$ ) variance for  $FC$ . The plotted values are weekly means calculated at 30-min temporal resolution from the flux time series. Vertical dashed lines represent, from left to right, the harvest dates of the crops in 2023, for rapeseed (13 July 2023), barley (22 August 2023) and corn (26 September 2023); and in 2024, for rapeseed (15 July 2024), barley (5 August 2024) and corn (13 September 2024). Dashed areas correspond to the 2023 harvest period (grey), the winter period (yellow) and the 2024 harvest period (purple), for a better comparison with Figure 5. Due to the two very long gaps in AF1 and AF3 (see Fig. [224](#)), plus some shorter gaps, there were no data corresponding to the harvest period in 2023 for  $FC$  or  $LE$  and only few weeks of data in the winter period. Note the logarithmic scale in panel (a), introduced due to the large magnitude of some of the CVs of  $FC$  for visualization purposes. [No gap-filled data were used to create this plot.](#)

534 [Figure 7 shows the effect size time series, based on the daily sums, The effect size \( \$d\$ \) values were larger in the case of the](#)  
 535 [comparison of  \$LE\$  sums than](#) for the comparison of  $FC$  and  $LE$  across the AF and between AF and MC. In the case of the AF

536 ~~evaluation for  $FC$  sums (Fig. 7). The values calculated using only the random error as the error in the measured data (Fig. 7a)~~  
537 ~~were larger than the values calculated inserting random plus systematic error as the error in the measured data (Fig. 7b). This~~  
538 ~~is a direct consequence of the inclusion of a larger denominator in Equation 3.~~

539 ~~In regard to effect size,  $d$  values were lower in 2023 than in 2024,  $d_{AF-FC}$  values were mostly in the range  $-0.7$  to  $-1.0$  in~~  
540 ~~most periods. After May in both years, values started to reduce progressively, reaching  $-1.3$ . The values were lowest (more~~  
541 ~~negative) of around  $-1.4$  in July 2024. With respect to the comparison between AF and MC for  $FC$ , the dynamics and  $LE$  and~~  
542 ~~in both error cases being considered. For  $FC$ , the values of  $d_{AF-MC-FC}$  were similar to the behavior  $AF-MC-FC$  were larger than~~  
543 ~~the values of  $d_{AF-FC}$ , with slight differences. The values were always between  $0.5$  and  $1.5$ , being especially concentrated in the~~  
544 ~~range  $0.8-1.0$  in the periods of February to May 2023, winter 2023/24, and March, August and September of 2024. In both~~  
545 ~~summers of 2023  $AF-FC$  in both years, and 2024, increased at the end of the growing season and during the harvest period in~~  
546 ~~2024. In the case of  $LE$ , the values of  $d_{AF-MC-FC}$  was larger with values between  $1.0$  and  $1.5$ . The maximum values were reached~~  
547 ~~in July 2023.~~

548 ~~The comparison of  $LE$  showed different dynamics (Fig. 7). Regarding the evaluation of  $AF-MC-LE$  were lower than the values~~  
549 ~~of  $d_{AF-LE}$ , the values were very constant at around  $-1.0$  during  $AF-LE$  in 2023 and winter 2023/24. In, but larger in 2024. The~~  
550 ~~largest values of  $d$  were attained during July, August and September of 2024, a higher variability was observed, but reduced~~  
551 ~~magnitudes (less negative) as compared to  $d_{AF-FC}$ . The magnitudes decreased slightly to  $-0.7$  to  $-0.8$  at for  $LE$  (magnitudes up~~  
552 ~~to 28), while in the case of  $FC$  values were largest at the end of the campaign, during the months of June, July and September~~  
553 ~~2024, while August showed again values close to  $-1.0$ . With respect to  $d_{AF-MC-LE}$ , values were in growing season in 2023~~  
554 ~~(magnitudes up to 12). The values of  $d$  for  $LE$  were larger than for  $FC$  in all periods except for the end of the growing season~~  
555 ~~of 2023, in the case of considering only random error (Fig. 7a). In the range  $0.7-1.1$  most of the time, with a slightly higher~~  
556 ~~variation from March to July 2023. During the 2024 growing season, the variability was lower. In general,  $d_{AF-MC-LE}$  varied~~  
557 ~~less than  $d_{AF-MC-FC}$  during the whole campaign. case of considering random and systematic errors (Fig. 7b),  $d$  values were~~  
558 ~~larger for  $FC$  in 2023 and for  $LE$  in 2024.~~

## 559 4 Discussion

### 560 4.1 Spatial and temporal variability of $FC$ and $LE$ above the AF system

561 Using three distributed EC stations over the same AF system, a small spatial variability in meteorological parameters was  
562 found, but the spatial variability in  $CO_2$  and energy fluxes was larger. ~~The AF site is not very large ( $19.1$  ha) compared to~~  
563 ~~the median farm size of  $29.4$  ha in Lower Saxony (?). The effect of several Several rows of trees perpendicular to the wind~~  
564 ~~can significantly influence the microclimatic conditions of different areas in the agricultural field main wind direction may~~  
565 ~~potentially influence microclimatic conditions across the AF, compared to open croplands (?). However, the meteorological~~  
566 ~~conditions (Kanzler et al., 2019), but this AF site ( $17.3$  ha) is smaller than the median farm size ( $29.4$  ha) in Lower Saxony~~  
567 ~~(Jänicke et al., 2022) and the meteorological variables were measured at the ~~three towers were very similar, probably due to~~~~  
568 ~~the fact that all stations were AF stations located within the tree strips, and not in between or outside them and due to the~~

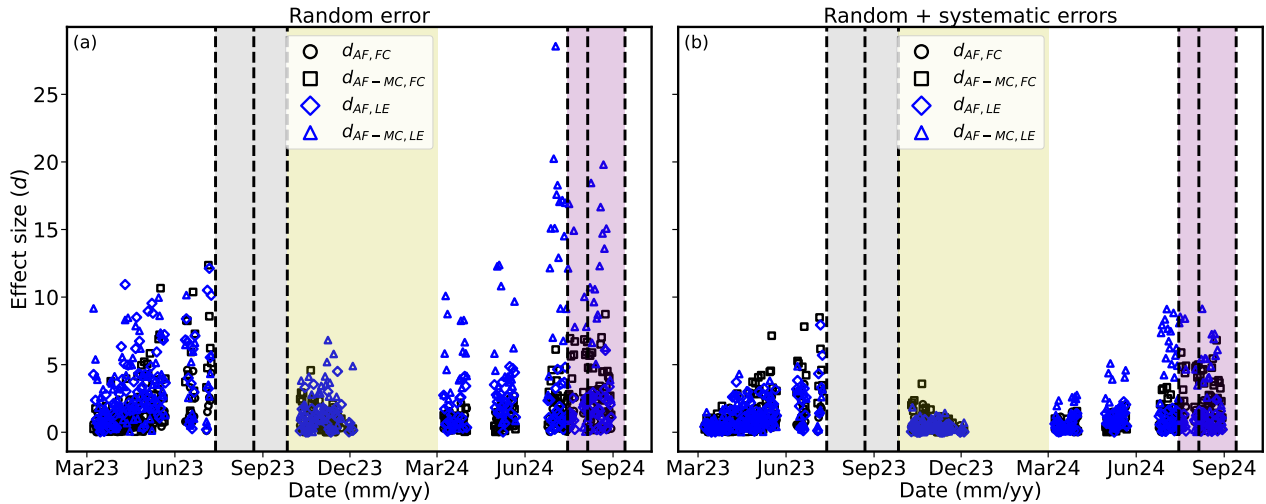


**Figure 7.** Time series of the effect size ( $d$ ) for  $FC$  and  $LE$ , using as the error in the measured data the random error (a) or the sum of random and systematic error (b).  $d$  was calculated according to Eq. 3, based on the daily sums of  $FC$  and  $LE$ . Time series of  $FC$  and  $LE$  had been filtered and gap-filled as described in section 2.3.3, and gaps with a duration over two weeks were excluded from the analysis. Black filled circles represent the comparison between AF1 and the average of the three stations at the AF (AF1, AF2 and AF3) for the  $FC$ . Black crosses represent the comparison between the average of the three stations at the AF (AF1, AF2 and AF3) and the MC-OC station for  $FC$ . Blue filled circles represent the comparison between AF1 and the average of the three stations at the AF (AF1, AF2 and AF3) for  $LE$ . Blue crosses represent the comparison between the average of the three stations at the AF (AF1, AF2 and AF3) and the MC-OC station for  $LE$ . Vertical dashed lines represent, from left to right, the harvest dates of the crops in 2023, for rapeseed (13 July 2023), barley (22 August 2023) and corn (26 September 2023); and in 2024, for rapeseed (15 July 2024), barley (5 August 2024) and corn (13 September 2024). Dashed areas correspond to the 2023 harvest period (grey), the winter period (yellow) and the 2024 harvest period (purple), as in Figure 6.

small size of the AF field. The-. These two factors can explain the low variability in meteorological parameters. Therefore, the observed variability in  $FC$  and  $LE$  should therefore not be attributed to the meteorological drivers, but to the rather to differences in the footprint areas of the three stations. The footprint climatology of the stations partially overlapped (Fig. 3), but the most intense flux contributions originated from an a small area around the towers. Differences in crop development and management practices could explain most of the spatial variability of the observed fluxes across the three towers throughout the campaign, because of the different crops that were sown in sown between the tree strips (spatial variability) and the different crop distribution from 2023 to 2024 (temporal variability) (Fig. 1).

The higher spatial variability in turbulent fluxes compared to other turbulence and wind parameters (Fig. 5), especially for  $FC$  and  $LE$ , was found also in the studies of ?-and-?Katul et al. (1999) and Oren et al. (2006). This can be explained by the control of stomatal and boundary layer conductances, as well as the more complex nature of sources and sinks for  $CO_2$  and  $H_2O$  fluxes (?). The (Katul et al., 1999) and the effects of landscape heterogeneity (Bou-Zeid et al., 2020). The explanation for

580 the spatial variability in the fluxes is the land cover attribution thanks to the footprint modeling, however other effects of the  
581 heterogeneity were not studied.

582 The larger CVs of FC at the eastern wind sectors (Fig. 5) during all evaluated periods relate directly to  
583 climatology differences differences in footprint climatology, because the footprints were the most different differed most at  
584 the eastern side of the three AF stations (Section 3.2). There was still a relatively large variability in LE and FC, due to the  
585 much smaller size of the footprint climatology area, which led to less overlapping footprints from the three stations (Fig. 5  
586 and 3), therefore higher, especially for the 50 % footprint climatology (Section 3.2). The harvest events in 2024 did not seem  
587 to affect have a big impact on the CVs (Figs. 5 and 6a) compared to the 2024 growing season, but they slightly reduced the  
588 variance magnitude (Fig. 6b and c).

589 The larger temporal variance, compared to spatial variance, for both *FC* and *LE*, could be explained by the **dominance**  
590 of seasonal and diel patterns of these variables. Spatial variability was important (seasonal and diurnal flux variability, which  
591 was more relevant than spatial variability (see Sections 3.4.1 and 3.4.2), but it had less relevance than the larger seasonal and  
592 diurnal variability. Nonetheless, Nevertheless,  $\sigma_t$  was similar to  $\sigma_s$  in winter for both *LE* and *FC*, which can be attributed to  
593 the dormant state of the ecosystem, leading to small diel variations and therefore diurnal variations and consequently small  
594 temporal variations. In summer 2024, for *LE*,  $\sigma_s$  was similar to  $\sigma_t$ , due to the less overlapping areas caused by a reduction in  
595 the lower area overlap caused by smaller footprints (Fig. 3) compared to the 2023 growing season, but also. This was also due  
596 to the absence of a fully developed crop in the eastern part of the field, because of the bad growth of rapeseed poor rapeseed  
597 growth during this season. This caused resulted in weaker LE measured, especially at tower AF1, and led to a lower spatial  
598 variation.

599 Compared In comparison to similar approaches in the literature, Peltola et al. (2015) found a paired temporal and spatial  
600 variability in  $\text{CH}_4$  fluxes measured at three different heights at on a tall EC tower and two additional EC stations over an  
601 agricultural landscape. Hollinger et al. (2004) measured fluxes using two towers with non-overlapping footprints in a forest  
602 and found that the temporal variability was larger, but; however, the spatial disagreement in *FC* was not negligible, despite  
603 the apparent homogeneity of the ecosystem studied. studied ecosystem. Rannik et al. (2006) also compared *FC* measured  
604 from two nearby towers over the same ecosystem, with partially overlapping footprints, and found relevant systematic errors  
605 in the daytime fluxes attributed to the variability in the turbulent flow field caused by the complexity of the terrain. These  
606 systematic differences were important to attribute for attributing long-term uncertainties in the ecosystem C uptake, such as it  
607 would happen ecosystem carbon uptake, as would be the case in the complex AF site of the present study. Davis et al. (2010)  
608 investigated heterogeneity in *FC* above an arable land and demonstrated the large imprint significant impact of spatial hetero-  
609 geneity in annual balances of C. Moreover, on annual carbon balances. Furthermore, Soegaard (2003) quantified the annual  
610 carbon budget of an agricultural landscape by combining footprint-weighted fluxes and spatial variability in different crops,  
611 demonstrating the large potential of spatial heterogeneity to bias annual estimates of fluxes flux estimates. In the present study,  
612 the influence of the different land covers around the towers was detectable for both FC and LE, except during the winter period;  
613 both for FC and LE, but. However, the differences were smaller than expected for different crops with clearly different season-  
614 ality. This could be explained by As other effects of heterogeneity on flux measurements cannot be captured with this setup, a

615 ~~first explanation could be~~ the partially overlapping footprints ~~, as already mentioned, but also to~~ and the buffering effect caused  
616 by the presence of the trees. ~~Trees~~ As trees were assumed to behave similarly across the AF, ~~so~~ their similar CO<sub>2</sub> and water  
617 fluxes attenuated the potentially ~~largest~~ larger differences in turbulent fluxes that would be expected among the crops without  
618 trees.

619 The observed variations in the weekly cumulative sums of *FC* and *ET* across the campaign (Fig. ~~??~~4) can be ~~explained by~~  
620 ~~the differences in the phenological state of the crops and the management around the towers~~ attributed to the developmental and  
621 management differences among the crops cultivated around the stations, provided that the trees were growing similarly across  
622 the entire AF site. These differences can be directly connected to the previously explained behavior of the *CVs* and partitioning  
623 of the variance. Spatially replicated experiments demonstrated the potential to more accurately estimate the uncertainty in  
624 turbulent fluxes, ~~such as applied in ?~~. ~~However, the footprint areas of the three stations at the AF e.g. by using non overlapping~~  
625 paired towers as in Hollinger and Richardson (2005), but this could not be applied in the present study ~~were not homogeneous~~  
626 ~~and they only partially overlap, which means that in practice it is difficult to assess the uncertainty for paired observations~~  
627 ~~as in ?~~ due to the overlapping footprints. Conversely, the deployment of three towers provided a more comprehensive dataset  
628 compared to the single tower approach, ~~and the uncertainty of the AF as a whole could be estimated by calculating the standard~~  
629 ~~deviation of the measured fluxes across the three towers~~. However, the ~~selection of the exact site of the towers~~ choice of  
630 the towers location in the present study might not have been optimal (~~?~~) (Chen et al., 2011), since footprints were partially  
631 overlapping (Fig. 1 and 3). This was due to logistic constraints that precluded the selection of any other location within the AF  
632 site, such as in the southernmost part of the field. On the other hand, the purpose of the study was to investigate ~~small-scale~~  
633 small-scale variability in the highly heterogeneous AF, a goal that was generally accomplished.

634 ~~Assuming that the trees were growing in a similar way across the whole AF site, the observed variations in weekly sums~~  
635 ~~of carbon and ET (Fig. ??) can be attributed to the developmental differences among the crops cultivated around the stations.~~  
636 Specifically, the earlier development of rapeseed in 2023 led to an initial carbon uptake at AF3, because the main footprint  
637 covered rapeseed (Fig. 3a). This ~~aligned with~~ matched the larger *CVs* of *FC* in the eastern side of the field (Fig. 5), and during  
638 March and April 2023 (Fig. 6a). However, the earlier growth of rapeseed did not ~~result in increased~~ increase *ET* in AF3 (Fig.  
639 ~~??~~4b), leading to comparable *CVs* of *LE* for all wind sectors (Fig. 5). This is because rapeseed can maintain a relatively large  
640 carbon uptake while using limited water resources (~~?~~) (Najibnia et al., 2014). The subsequent development of corn and barley  
641 led to similar weekly uptakes of carbon at AF1 and AF2, but a larger *ET* at AF1, leading to a decrease in the *CVs* of *FC* and a  
642 modest increase in the *CVs* of *LE*. Besides the partially overlapping footprint (Fig. 3), ~~the reason behind is the~~ another reason is  
643 a different water use efficiency among barley and corn, being lower for barley and therefore explaining similar carbon uptake  
644 as corn at a higher *ET* (see e.g. ~~?~~ Pohanková et al., 2018). After the short drought in May-June, which affected all three stations  
645 by reducing both carbon uptake and *ET* ~~due to water stress~~, weekly carbon uptakes of AF1 and AF2 and weekly *ET* sums  
646 were larger than for AF3 until the harvest period. This can be attributed to corn and barley being less present in the footprint  
647 area of AF3 (Fig. 3a). Corn and barley exhibited a more intense physiological activity, immersed in the growing season, while  
648 rapeseed was likely at its maturity stage.

649 The ~~harvest-of-rapeseed-rapeseed harvest~~ in 2023 had a negligible effect on the carbon uptake of AF1 and AF2 much, but  
650 seemed to have an effect on *ET*, which reduced for both stations. This can be attributed to a period of several precipitation  
651 events, low *TA* and *VPD* (Fig. 2) which reduced both physiological activity and atmospheric water demand. The ~~harvest-of~~  
652 barley and corn harvests reduced the carbon uptake and *ET*. Especially the corn harvest had a large impact because it was  
653 the main crop in the footprints of AF1 and AF2 (Fig. 3b). After the harvest period, the slightly larger difference between the  
654 three stations may be an effect of the larger gap-filling uncertainty due to the longer gaps and agrees with an enhanced spatial  
655 variance compared to the temporal ~~one-variance~~ (Fig. 6b and c).

656 In 2024, the very dry spring (Table 2) did not affect weekly sums of *ET* ~~since they were similar to the previous year, but~~  
657 ~~affected, but reduced the magnitude of~~ weekly sums of *FC* ~~visible by lower fluxes~~ compared to 2023. In 2024, there was no  
658 earlier development of the rapeseed as it occurred in 2023, due to the very wet winter conditions. The variability in *ET* was  
659 larger than in 2023 due to less overlapping footprints and due to the difference in rapeseed growth (Fig. 3d). The larger carbon  
660 uptake at AF2 as well as larger *ET* (Fig. ??) ~~during all the 2024 growing season was due to 4)~~ during the whole growing season  
661 of 2024 can be explained by the influence of barley and partially corn, while AF1 detected only part of the barley field and the  
662 non-well developed rapeseed (Fig. 3c). Carbon uptake and *ET* were smaller at AF3 because corn developed later, but reached  
663 similar values as AF1 once corn started to grow. After the ~~harvest-of-the-rapeseed-rapeseed harvest~~, AF1 and AF2 reduced both  
664 their carbon uptake and *ET* release, with AF2 turning into a carbon source. ~~The effect was more intense for AF2, This was~~  
665 explained not by the footprint of AF2 in the rapeseed field (Fig. 3e), but rather by the ~~fact that barley had reached the maturity~~  
666 ~~already and there was a mature barley and the~~ strong ecosystem respiration ~~enhanced due to the rainy and wet conditions, as~~  
667 ~~well as a reduced ET under wet conditions~~. Carbon uptake and *ET* release at AF3, on the other hand, did not detect the effect  
668 of the rapeseed harvest, because AF3 was not measuring the corresponding portion of the field (Fig. 3e). AF3 kept a large  
669 weekly carbon uptake and similar *ET* due to the presence of the corn in its footprint area (Fig. 3). Afterwards, the ~~harvest-of~~  
670 ~~barley-barley harvest~~ reduced the uptake of AF1, turning it onto a carbon source, and of AF3, as well as *ET* due to the footprint  
671 covered by both stations (Fig. 3e). ~~FC was progressively more positive at all three towers until it reached carbon emissions also~~  
672 ~~for AF1 and AF3 around the harvest of the corn~~ Carbon uptake progressively reduced until it eventually turned to emissions  
673 around the corn harvest, which was the main crop in the footprint area of AF3.

#### 674 4.2 Differences in *FC* and *ET* between AF and ~~MC~~ OC systems

675 The AF site had typically lower air temperature and higher *RH* than the ~~MC~~ OC (Fig. 2), because the trees at the AF act  
676 as a buffer to keep cooler air temperatures and cooler soil resulting in a larger *RH*. This is pointed out in a review by ?  
677 Quandt et al. (2023). The authors stated that during drought events and under drier and warmer climatic conditions, as projected  
678 in future climate scenarios, ~~the buffer effect of the trees in keeping trees might potentially help in sustaining~~ cooler temperatures  
679 and ~~more humid air could potentially be enhanced~~ the air more humid.

680 ~~C~~ Carbon uptake and *ET* release were enhanced at the AF at the beginning of the 2023 growing season, because of the  
681 earlier development of the trees and the rapeseed, both present in the footprint of all three AF stations (Fig. 1 and 3a).  
682 ~~The MC, while the OC~~ station was measuring mostly ~~the corn field corn~~ (Fig. 3a). Corn is a crop with a later develop-



ment compared to barley or rapeseed (~~??~~), but (Lokupitiya et al., 2009; Soegaard, 2003), but is typically very productive (~~??~~) (Hollinger et al., 2005; Lokupitiya et al., 2016). Therefore, carbon uptake was larger at the MC-OC during most of the 2023 growing season after corn started ~~its stronger development phase~~ to grow, later than rapeseed and barley. A similar ET ~~on the other hand, was similar to~~ between OC and AF2 ~~indicating~~ (Fig. 4b) indicated a larger water use efficiency at the OC. In our study, the short dry period in May/June 2023 ~~occurred when the corn was at its highest development stage. Therefore the corn was not affected as strongly as the~~ took place before corn reached its peak growth stage, while rapeseed and barley ~~which was were~~ in a more advanced ~~development stage~~ stage and were more affected by the dry conditions. In general, the whole campaign took place during very wet conditions, ~~which potentially enhanced~~. This might have increased the ecosystem respiration ~~due to the fostered~~ because it led to more soil organic matter decomposition ~~with~~ driven by larger litter amounts at the AF. This, together with a larger respiration from the trees, can explain why AF2, ~~although being even though it was~~ surrounded by corn, did not ~~show similar carbon uptake, take up as much carbon~~ as the other ~~tower within towers in~~ the AF system.

During the 2023 harvest period, the footprint of the ~~MC station covered only~~ OC station was limited to corn, not rapeseed (Fig. 3b). Corn ~~was still growing during~~ continued to grow in July and August of 2023 at the MC-OC, which explains why at the ~~MC tower~~ OC a very large carbon uptake and *ET* release was ~~retained~~ observed, while AF2 and AF1 showed reduced fluxes. In winter ~~carbon and ET weekly sums were very similar, due to the dormant state of the ecosystems as mentioned in the previous section, the ecosystems were dormant which explains the small differences between AF and OC~~. However, fluxes were very small in magnitude and it ~~is difficult to attribute clear~~ was difficult to observe differences between sites.

During the 2024 growing season, carbon uptake at the AF-OC was similar to the ~~MC, which is different to 2023. The magnitude of the carbon uptake at all stations was lower than AF, but ET was larger at the OC, opposite to what occurred in 2023. In 2024, barley was~~ This could be explained by barley grown in the main footprint area of the MC-OC (Fig. 3d), as well as a portion of the rapeseed field, which did not grow well this year. ~~In general, barley~~ Barley is a crop with less intense physiological activity ~~than corn (?), which~~ and lower water use efficiency than corn (Pohanková et al., 2018). This explains the smaller differences to the AF stations in C uptake and a much larger ET. Also, the meteorological conditions were very wet in winter with a dry spring. During the harvest period in 2024 the carbon uptake and *ET* reduced more sharply at the MC-OC than at the AF, after the ~~harvest of the rapeseed~~ rapeseed harvest, because of its partially contributing footprint (Fig. 3e). The reduction was more pronounced after the ~~harvest of the barley~~ barley harvest, which contributed the most to the ~~main~~ footprint covered by the station.

~~Trees within the AF buffer all the effects of management practices of the crops in between tree strips, since their eco-physiological activity follows a clear seasonality, similar to forests in comparable climates (?), and might partially mask the effect of management in certain portions of the field. Since all three towers at the AF cover similar footprint areas and the western side of the stations was always predominant in the footprint climatology, only large changes in the source/sink behavior of the field around them can be detected. During the 2023 growing season the footprint area contributing to the fluxes (Fig. 3) covered corn, which was harvested at the end of September, so just a small effect on the fluxes was observed after the harvest~~

717 of the barley at the end of August (Fig. ??). In 2024, on the other hand, the effect of harvest on a reduction in carbon and *ET*  
718 was more pronounced, because of the earlier development of barley compared to corn.

719 By contrast, in the paper by ?, the authors compared 4 months of measurements and both carbon uptake and *ET* were  
720 enhanced at the AF during a measurement campaign from April to August 2022, conducted at the same site. Similar results  
721 were obtained by ?, who showed an enhanced carbon uptake and *ET* release at a grassland AF system compared to a MC  
722 grassland. However, they only measured in summer, with enhanced physiological activity of grasses and trees. The dominant  
723 species in the footprint area of the MC stations were rapeseed in ? and grass in ?. These species are known to have a lower  
724 physiological activity as compared to corn (??).

### 725 4.3 Effect size and spatial representativeness of the distributed network

726 The effect size  $d$  ~~was in most cases~~ is a measure of the relative difference of two variables for two different populations (in this  
727 case two ecosystems or towers within an ecosystem) with respect to the pooled standard deviation of the two populations. The  
728 interpretation of the calculated values was done according to Figure 3 in the paper by Hill et al. (2017), where the number of  
729 EC replicates over an ecosystem or for comparing two ecosystems was estimated based on the desired statistical power (from  
730 0 to 1) and the effect size value. The statistical power related to the confidence in the accuracy of the measurements, such that  
731 a value of 1 means we can be 100 % certain about the measured differences.

732 In the case of comparing the AF, similar values for both *LE* and *FC* were attained, mostly between 0 and 5. Values of 5  
733 meant that with three towers a statistical power between 0.7 and 1.3 (Fig. 7), indicating differences between the evaluated  
734 daily sums of *FC* and *ET* on the order of the pooled standard deviation, therefore leading to a relatively large effect size (?).  
735 The lower variability of 0.95 was achieved, however with values close to 0, the statistical power dropped dramatically so no  
736 confidence in the accuracy of the differences could be drawn. In the case of comparing AF-MC,  $d$  for *LE* than for *FC* across  
737 the whole measurement campaign relates directly to the findings discussed in previous sections, e.g. the *FC* had the largest  
738 spatial variability most of the time. Larger spatial variation in *FC* influences daily sums which were later on used to calculate  
739  $d$ . The increase in spatial variability of *FC*, which was more pronounced than the change in spatial variability of *LE*, explained  
740 the increase in  $d$  during the growing seasons of 2023 and 2024, for both values were larger than for the comparison of AF vs.  
741 MC and the comparison of the three stations at the AF.

742 The larger  $d$  values calculated for the comparison between AF and MC than for the comparison between multiple towers at  
743 the AF (Fig. 7) can be interpreted as an effect of the larger ecosystem differences between AF and MC than within the AF. The  
744 differences within the AF system were a result of the small-scale heterogeneity of the AF system. Because differences in means  
745 were larger than differences in the standard deviation,  $d$  can be interpreted such that a network of three EC towers above the  
746 AF allowed a better understanding of the effect of management and smaller scale disturbances inside the AF system. However,  
747 at the ecosystem-scale comparison, AF vs. MC, the traditional approach with only one EC tower could still be sufficient to  
748 detect differences between the two ecosystems.

749 Low values of  $d$  were typically attained during winter months. Then fluxes were small the AF, which meant that a larger  
750 statistical power was achieved because the daily sums were larger than the pooled uncertainty. Values larger than 2 or 3 in

many cases, reaching up to 15 or 20, meant a statistical power above 0.975, therefore a very large confidence in the daily sums. Furthermore,  $d_{LE}$  was larger than  $d_{FC}$ , meaning that the statistical confidence was larger for *LE*. When using random and systematic errors as the errors attributed to measured data (Fig. ??), which lead to a decrease of both the temporal and spatial variability (Fig. 5 and 6) 7b),  $d$  values were much lower. This matches the interpretation of Hill et al. (2017): if the EC systems are too uncertain, the number of systems needed to achieve a large statistical power (above 0.9) increases exponentially. If the LC-EC setups used in this study would be a lot less accurate, e.g. with two times more systematic error compared to conventional EC, the effect size values would be too low so no certainty about the data could be ensured, unless the number of towers would increase according to counteract the loss of accuracy. The small effect of heterogeneity across the sites was likely masked by the larger noise in the data, the longer and more frequent gaps and the larger uncertainty in the gap-filled fluxes (Section 2.3.3).

Several studies addressed the spatial representativeness of fluxes and the footprint climatology. These studies focused either in studying RE (?), in on studying RE (Hollinger and Richardson, 2005), on separating ecosystem structure and sampling errors in the spatial variability of fluxes (?), in (Oren et al., 2006), on disentangling temporal and spatial variability of fluxes using a single tower approach and footprint modeling (??), in (Levy et al., 2020; Soegaard, 2003), on the representativeness of single point measurements at the pixel scale for regional to global scale models (????), or in (Chasmer et al., 2009; Chen et al., 2009; Wang et al., 2024), or on studying the effect of diverse meteorological conditions in the footprint climatology and canopy structure (?)(Abdaki et al., 2024). To the best of our knowledge, the study of ? Cunliffe et al. (2022) was the only one deploying that deployed several LC-EC setups, similar to the ones similar to those used in our study, and one additional conventional EC setup, to quantify the impact of landscape heterogeneity on turbulent fluxes. They studied a dryland site with very low flux magnitudes, which is different from our site, and. They obtained a useful agreement between different LC-EC and the conventional EC setups. The and attributed the differences between setups were attributed to the heterogeneity of the ecosystem to the ecosystem heterogeneity, covered by different bushes and grass species, but. However, a less detailed analysis on the spatial and temporal variability of the fluxes was performed.

In the EC community, EC replicates are not common(?). Therefore uncommon (Hill et al., 2017; Stoy et al., 2023). Therefore, the effect size of either means or sums of fluxes is typically not estimated. ?Hill et al. (2017), as the first paper showing the potential of LC-EC setups in increasing spatial replication in EC studies, estimated the effect size through the comparison of the by comparing the average carbon sequestration and the standard deviation of the cumulative sums, for ideal and non-ideal FLUXNET sites (?)(Baldocchi, 2014). In the present study, the effect size was calculated in a similar waysimilarly, but based on daily sums and pooled standard deviations (errors) of the 30-min time series. The concept in ?, therefore, was different, since the Hill et al. (2017) was different since measurement errors tend to decrease relative to the aggregation period when cumulative sums are calculated (?)(Moncrieff et al., 1996). Their calculated standard deviation was based on the uncertainty in the cumulative sums of the half-hourly carbon fluxes and not, rather than on time series of with a higher temporal resolution, e.g. (30 minutes). These time series are commonly characterised characterized by higher variability. Due to this difference in the time scale used in the analysis, their findings on how many towers are needed to properly sample an ecosystem cannot be compared to ours, and a potentially lower effect size.

In general, there is still an ongoing discussion on how much the landscape heterogeneity affect balances of  $\text{CO}_2$ -carbon and  $\text{H}_2\text{O}$  measured by single EC towers. The LC-EC setups could help to bridge the gap of low spatial replication across such heterogeneous sites by allowing the installation of multiple setups due to their reduced cost. This could be complementary to other methodologies developed, to understand the effect of spatial heterogeneity on fluxes measured from single towers, such as in ~~or~~ Levy et al. (2020) or Griebel et al. (2016), or measured with several conventional EC setups (Soegaard, 2003; Hollinger et al., 2004; Katul et al., 1999; Oren et al., 2006).

#### 4.4 Footprint modeling Heterogeneity as a challenge to EC measurements and turbulence dynamics at the AF site footprint modeling

The footprint model employed in the present study (~~?~~) allowed to understand where the source/sink areas of  $\text{CO}_2$  and  $\text{H}_2\text{O}$  were located. As mentioned in the introduction, the heterogeneity in the surface properties of a certain ecosystem induces horizontal advection, secondary mesoscale circulations and non-equilibrium turbulence processes (Bou-Zeid et al., 2020). Horizontal advection at different spatial scales can distort flux measurements (Cuxart et al., 2016). Furthermore, the dynamics of the roughness sublayer (RSL), defined as the atmospheric layer influenced by the roughness elements and located below the inertial sublayer (Katul et al., 1999), can be modified by the wind barrier of trees in the AF (van Ramshorst et al., 2022). Upon a change in the underlying surface, an internal equilibrium layer (IEL, Brutsaert 1998) and an internal boundary layer (IBL, Garratt 1990) develop. Multiple IELs and IBLs can develop if there are multiple transitions in the surface, such as at the AF (Bou-Zeid et al., 2020). At the AF, the major change in the surface is represented by the tree rows (Markwitz, 2021). These rows create persistent waves that enhance the differences in the turbulence-related parameters  $WS$ , at a basic level. The implementation of the aerodynamic canopy height after ~~?~~ helped to increase the accuracy of the footprint model to cope with the heterogeneity of the AF site. The ~~USTAR~~, and ~~W SIGMA~~, though these changes are less pronounced than flux variations. Furthermore, the classical tests of stationarity and equilibrium may fail if the EC station is placed above the IEL (Mahrt and Bou-Zeid, 2020), due to a disequilibrium between the mean flow, turbulence and the new surface (Bou-Zeid et al., 2020). Additionally, the complex canopy structure at the AF could lead to significant carbon and energy storage, particularly at the crop-tree interfaces and within the dense tree rows. These storage terms may influence advection in the horizontal and vertical directions (Mammarella et al., 2007; Aubinet et al., 2010; Feigenwinter et al., 2008). These effects may affect the turbulence and flux measurements, however they could not be quantified with the current setup.

The footprint size and the overlap between footprints decreased between 2023 and 2024 due to tree growth (Fig. 3). Combined with changes in crop development and meteorological conditions, this increased the spatial components of the variance for  $FC$  and  $LE$  (Fig. 5). While the three towers at the AF shared a similar footprint climatology had partially overlapping 80 % footprint climatology areas (Fig. 3), if the 80 or 90 % area of the contributions to the footprint were considered. However, the most intense footprint values, which indicate the largest contribution to the measured fluxes, concentrated in smaller areas around the towers (~~?~~) the main footprint contributions concentrated in the immediate areas around each tower (Kljun et al., 2002). Therefore, most of the observed variability in the development of  $FC$  and  $LE$  flux variability can be attributed to the heterogeneity in the land cover land cover differences around the stations, with different crops at different

phenological stages during the campaign. The smaller variability of fluxes in winter can be attributed to the absence of crops and the latency state of the trees. One of the key features of the three towers network is that it allowed to disentangle the effect of management activities (e.g. crop harvest) and provided insights into small-scale features caused by the alternating structure of the AF. The division of data in the data into wind direction bins, as done in e.g. Kutsch et al. (2005), to address the spatial variability of fluxes, turbulence parameters and both spatial variability in fluxes and turbulence parameters, as well as the spatial and temporal components of the variance, complemented the information provided by the footprint maps.

Canopy height influences the wind speed and the dynamics of turbulence within the AF (?), and therefore the footprint covered by the towers (?). The footprint area, therefore, is very sensitive to a steep change in the canopy elements. The increase in tree height from 2023 to 2024 led to a reduction of the footprint size and less overlap between them (Fig. 3). This, together with differences in crop development and meteorological conditions, contributed to an increase in the CVs of  $FC$  and  $LE$ , and showed the relevance of the spatial components of the variance for both flux variables.

The parameterization implemented in the model of ? does not allow to consider the effect of the footprint model used in the present study (Kljun et al., 2015) allowed to understand, at a basic level, where the source/sink areas of  $CO_2$  and  $H_2O$  were located. Nevertheless, the parametrization of the footprint model does not consider the effects of spatial heterogeneity as represented by on the basic parameters roughness length and  $U_{STAR}$ , which are the basic parameters for an accurate footprint estimation. This is the main source of uncertainty for the footprint modeling in this study, nor how canopy heterogeneity influences wind speed and turbulence dynamics within the AF (Markwitz, 2021). Due to the structure of the AF, it is likely that the footprint model overestimates likely overestimated the footprint area, attributing the by attributing sources and sinks to areas further beyond what really contributes that do not actually contribute to the flux. In addition Additionally, footprint estimates are sensitive to the vertical distribution of sources and sinks along within the canopy and to the time air parcels spend within it (??) that air parcels spend within it (Launiainen et al., 2007; Prabha et al., 2008). This is likely happening at this AF site, due to the structure of the tree rows. A more advanced modeling approach combining, firstly, information on implementing the aerodynamic canopy height after Chu et al. (2018) helped to partially account for the heterogeneity of the AF site in the footprint modeling, but this procedure was also limited. More accurate footprint estimates could be obtained by combining flow dynamics and spatial structure, with e.g. information using Large Eddy Simulations, similar as performed in ? and ?, and secondly, footprint modeling by applying the procedure described in ? (Markwitz, 2021; van Ramshorst et al., 2022), with a more advanced footprint modeling as described in e.g. Göckede et al. (2006) to account for the spatial heterogeneity in roughness length and friction velocity, would provide more accurate footprint estimates. In addition, if  $U_{STAR}$ . Additionally, aggregating the footprint climatology were aggregated based on weighted footprints, as in ?, the sources and sinks of carbon and water vapour across the site would be characterized in more detail.

The structure of the AF system influences the flow dynamics and therefore affects the turbulence measurements. An Internal Boundary Layer develops across the field, due to the obstacle represented by the edge of the tree rows (?). In the roughness sublayer, tree rows induce persistent waves behind them, thereby enhancing the differences in the turbulence-related parameters  $WS$ ,  $U_{STAR}$ , and  $W_{SIGMA}$ . However, the dissimilarities were not larger than for the  $LE$  or  $FC$  (Fig. 5 and 6), because these

855 ~~were controlled by the very irregular distribution of~~ Chen et al. (2009), ~~would allow for a more detailed characterization of the~~  
856 ~~sources and sinks of carbon and water~~ sources/sinks, ~~which had a larger impact than the variability in turbulence statistics. In~~  
857 ~~addition, the canopy structure and the spatial heterogeneity at the AF could potentially lead to a large storage of carbon and~~  
858 ~~energy. The storage terms were not accounted for, although they might be relevant at the edges between crops and trees and~~  
859 ~~within the tree rows, which are very dense and therefore less coupled with the atmosphere. All of it might influence advection~~  
860 ~~in horizontal and vertical directions (???)~~, however, it was not possible to account for those terms with the current datasets.  
861 vapor.

862 Furthermore, the sensor location bias, defined as the uncertainty caused by measuring ~~only at~~ at only one point above  
863 a heterogeneous site, ~~also~~ depends on the stability conditions ~~(?)~~ (Chen et al., 2011). Under more unstable conditions, the  
864 footprint size ~~would decrease~~ decreases and the location bias of each ~~of the towers would increase~~, better justifying the use  
865 ~~of several tower increases. This justifies the use of multiple~~ EC towers to ~~better sample the whole ecosystem~~ sample an entire  
866 ecosystem more effectively. A more detailed study ~~on~~ of stability regimes, footprint size and spatial variability of fluxes would  
867 inform ~~on this feature, but it~~ about this feature. However, this was not performed in this study due to the limited data availability  
868 and to the difficulty in gap-filling turbulence parameters needed to classify stability regimes, such as Obukhov length. With  
869 longer time series and more complete turbulence and footprint information, some of the previously detailed shortness of this  
870 study could be addressed.

#### 871 **4.4.1 Errors in $FC$ , $LE$ and $H$**

872 ~~The errors that affect the flux calculation~~

#### 873 **4.5 Errors in $FC$ , $LE$ and $H$**

874 Errors affecting flux calculations are difficult to disentangle ~~as they propagate through the whole because they propagate~~  
875 ~~throughout the entire~~ processing routine, from ~~the~~ raw data measurements ~~until the~~ to final flux corrections. Therefore, the un-  
876 certainty in the ~~use of measured fluxes from the~~ LC-EC ~~was assigned, for the measured fluxes, setups was assigned~~ based on the  
877 random error and the previous inter-comparison studies of ~~?~~ and ? Callejas-Rodelas et al. (2024) and van Ramshorst et al. (2024)  
878 , as detailed in Section 2.5. This procedure is similar to the approach applied in ~~?~~ Peltola et al. (2015), where they used a pre-  
879 vious instrument cross-comparison campaign ~~(?)~~ (Peltola et al., 2014) to assign instrumental uncertainty to the setups they  
880 deployed. However, the uncertainty in the use of LC-EC, defined in relation to conventional EC, was obtained during a specific  
881 campaign and under specific site conditions ~~, hence~~ with the same footprint area; therefore, there might be a bias in the LC-EC  
882 error attribution. Additionally, as explained in Section 2.5, the uncertainty in the gap-filled fluxes was calculated ~~as explained~~  
883 ~~in Section 2.5~~, by assigning individual errors to the 30-min fluxes, which can then be propagated when performing the daily  
884 cumulative sums. This was detailed as ~~a first attempt on how to easily evaluate errors and propagate them~~ an initial method  
885 for easily evaluating and propagating errors through cumulative sums ~~whenever a new EC setup has been compared when~~  
886 comparing new EC setups to conventional EC setups and ~~balances of calculating~~ carbon or ~~ET~~ are calculated balances using



gap-filled data. Other approaches, as described in e.g. Richardson and Hollinger (2007), could potentially be applicable to this dataset as well.

~~Focusing on the uncertainty in the gap-filling procedure, the presence of~~ Including all gap-filled data, with some very long gaps, ~~especially affecting tower 3 at the AF~~ particularly affecting AF3, would have ~~had largely increased the uncertainty in the data (?) if all the time series were filled~~ made the analysis more uncertain (Lucas-Moffat et al., 2022). Therefore, only measured data and gaps shorter than two weeks were used, ~~which did not allow for a~~ although this did not permit a more complete spatial heterogeneity study, ~~mainly because of the missing data for AF3 during the harvest period 2023. Using the combination of both REddyProc for very~~ throughout the campaign. The optimal solution for this study was to use a combination of REddyProc ~~for~~ short gaps and the XGBoost model for long gaps ~~was the optimal solution found for this study, similar as done in ?, and it-, similar to what was done in Winck et al. (2023). This solution~~ allowed to assign individual errors to each 30-min flux, as explained in Section 2.5. Additionally, ~~using~~ applying more strict filtering criteria, such as a higher *USTAR*-threshold or a lower quality flag, would ~~on the one hand provide data of better quality, but would on the other hand increase the~~ provide higher-quality data but would also increase uncertainty due to ~~gap-filling of a higher number of the filling of more~~ gaps.

We used *TA*, *SW\_IN* and *VPD* as predictors for gap-filling, which are generally recognized as the main drivers of  $\text{CO}_2$  and  $\text{H}_2\text{O}$  fluxes ~~(??)~~ (Vekuri et al., 2023; Wutzler et al., 2018). *WS* was used because of its influence on ~~the development of turbulence and on turbulence development and~~ the spatial information carried by eddies, especially above a very rough surface, such as the AF ~~and wind.~~ Wind direction was selected to account for the spatial heterogeneity across the different measurement locations of the towers ~~(?)~~ (Richardson et al., 2006). Other meteorological variables were either less relevant for the analysis, such as atmospheric pressure, or more complex to gap-fill, such as net radiation.

~~Random error (RE) was not considered directly in this analysis, however, it was partially accounted for indirectly when calculating standard deviations of the time series. In addition, RE decreases with increasing length of the datasets (?), therefore it becomes less relevant for longer term assessment of carbon and ET balancees. Also, the approach implemented in e.g. ? and ? treated RE either with similar conditions in consecutive days, or with the approach of two independent towers, but in the present study the towers had partially overlapping footprints and different land covers around them, hence, cannot be considered as independent.~~

## 5 Conclusions

This study ~~shows~~ presents for the first time 1.5 years of measurements from a distributed network of three ~~EC~~ eddy covariance towers above a temperate heterogeneous agroforestry system ~~and, as well as~~ a comparison to an adjacent ~~monocropping, open cropland~~ agricultural system. ~~The use of three EC~~ Using three eddy covariance stations allowed to capture the spatial and temporal variability across the site, which ~~especially affected FC~~ particularly affected carbon flux. The main differences were attributed to the different developmental stages of the crops across seasons, with larger disturbances ~~of FC and LE in carbon flux and latent heat flux~~ after harvest events. ~~Because of~~ Due to the high degree of spatial heterogeneity, ~~it was important to have~~ a broader footprint coverage ~~to capture small scale~~ was necessary to capture small-scale differences at the AF agroforestry.

920 Furthermore, binning the data ~~in by~~ wind direction sectors and weeks ~~allowed us to have~~ provided a detailed picture ~~on of~~ the  
921 temporal and spatial components of the variance and the coefficients of spatial variation, ~~given that~~. This was important  
922 because the differences between ~~the different~~ stations were small enough to be masked ~~if by~~ a less resolved analysis ~~had been~~  
923 performed.

924 Secondly, this study ~~included~~ incorporated a complex gap-filling procedure ~~which that~~ complemented previously published  
925 recommendations on ~~how to work~~ working with lower-cost EC eddy covariance data. The datasets gathered during the cam-  
926 paign and the processing scheme added value to the data collection of the project, ~~from previous years of measurements, above~~  
927 from several agroforestry and ~~monocropping~~ open cropland sites. Future research will address ~~in more detail~~ the contrast  
928 between different agroforestry and ~~monocropping sites, with~~ open cropland sites in more detail, using more years of data ~~and~~  
929 under a broader range of meteorological conditions.

930 Finally, the footprint coverage required to capture the spatial heterogeneity across the AF agroforestry, and within the AF  
931 and MC agroforestry and open cropland, was improved ~~thanks to the use of by using~~ lower-cost EC eddy covariance setups. We  
932 ~~proved satisfactorily~~ satisfactorily proved the hypothesis that the degree of uncertainty introduced by ~~the use of using~~ slower-  
933 response gas analyzers for CO<sub>2</sub> and H<sub>2</sub>O was counteracted by the better representation of all processes occurring within  
934 the AF agroforestry system. Therefore, we recommend ~~the installation of multiple EC~~ installing multiple eddy covariance  
935 setups, including lower-cost setups, ~~anytime when whenever~~ the degree of heterogeneity of an ecosystem is large. ~~An added~~  
936 ~~value in future studies would be to compare~~ Future studies could benefit from comparing overlapping and non-overlapping  
937 measurements in terms of footprint.

938 *Code and data availability.* Data corresponding to this publication, as well as the codes to analyze results and prepare the figures for this  
939 publication are available at Zenodo, <https://doi.org/10.5281/zenodo.14855288> (Callejas-Rodelas et al., 2025).

940 *Author contributions.* JACR performed the measurements, data analysis and manuscript writing. AK and CM wrote the project proposal,  
941 contributed to data analysis and manuscript editing. IM, TV and OP contributed to data analysis and manuscript editing.

942 *Competing interests.* The authors declare that they have no known competing financial interests or personal relationships that could have  
943 appeared to influence the work reported in this paper.

944 *Disclaimer.* TEXT

945 *Acknowledgements.* We wish to acknowledge the funding agencies for providing the necessary funds to ~~run-out~~perform this research, as  
946 well as the technical support in the field work received by Marek Peksa, Frank Tiedemann, Edgar Tunsch, Dietmar Fellert, and student  
947 assistants (Bioclimatology group) from the University of Göttingen. We wish to acknowledge as well the support from the team of the  
948 Micrometeorology Group at the University of Helsinki and from ~~LUKE~~the Natural Resources Institute Finland (LUKE) in Helsinki.

949 *Financial support.* This research was supported by the German Federal Ministry of Education and Research (BMBF, project BonaRes,  
950 Module A, SIGNAL 031B1063A). This project also received funding from the European Unions' Horizon 2020 research and innovation  
951 program under Grant Agreement No. 862695 EJP SOIL, the German Academic Exchange Service (DAAD), and the Reinhard-Süring-  
952 Foundation (RSS), affiliated to the German Weather Society and ICOS-Finland by University of Helsinki. Olli Peltola acknowledges Research  
953 Council of Finland for funding (grant no. 354298).

- 955 Abdaki, M., Sanchez-Azofeifa, A., Vargas, R., Ludwig, R., and Hamann, H. F.: Spatial and Temporal Variation of  
 956 Three Eddy-Covariance Flux Footprints in a Tropical Dry Forest, *Agricultural and Forest Meteorology*, 345, 109863,  
 957 <https://doi.org/10.1016/j.agrformet.2023.109863>, 2024.
- 958 Aubinet, M., Feigenwinter, C., Heinesch, B., Bernhofer, C., Canepa, E., Lindroth, A., Montagnani, L., Rebmann, C., Sedlak, P., and  
 959 Van Gorsel, E.: Direct Advection Measurements Do Not Help to Solve the Night-Time CO<sub>2</sub> Closure Problem: Evidence from Three  
 960 Different Forests, *Agricultural and Forest Meteorology*, 150, 655–664, <https://doi.org/10.1016/j.agrformet.2010.01.016>, 2010.
- 961 Aubinet, M., Feigenwinter, C., Heinesch, B., Laffineur, Q., Papale, D., Reichstein, M., Rinne, J., and Van Gorsel, E.: Nighttime Flux Cor-  
 962 rection, in: *Eddy Covariance: A Practical Guide to Measurement and Data Analysis*, edited by Aubinet, M., Vesala, T., and Papale, D.,  
 963 Springer Netherlands, Dordrecht, <https://doi.org/10.1007/978-94-007-2351-1>, 2012.
- 964 Baldocchi, D.: Measuring Fluxes of Trace Gases and Energy between Ecosystems and the Atmosphere – the State and Future of the Eddy  
 965 Covariance Method, *Global Change Biology*, 20, 3600–3609, <https://doi.org/10.1111/gcb.12649>, 2014.
- 966 Böhm, C., Kanzler, M., and Freese, D.: Wind Speed Reductions as Influenced by Woody Hedgerows Grown for Biomass in Short Rotation  
 967 Alley Cropping Systems in Germany, *Agroforestry Systems*, 88, 579–591, <https://doi.org/10.1007/s10457-014-9700-y>, 2014.
- 968 Bou-Zeid, E., Anderson, W., Katul, G. G., and Mahrt, L.: The Persistent Challenge of Surface Heterogeneity in Boundary-Layer Meteorology:  
 969 A Review, *Boundary-Layer Meteorology*, 177, 227–245, <https://doi.org/10.1007/s10546-020-00551-8>, 2020.
- 970 Brutsaert, W.: Land-Surface Water Vapor and Sensible Heat Flux: Spatial Variability, Homogeneity, and Measurement Scales, *Water Re-*  
 971 *sources Research*, 34, 2433–2442, <https://doi.org/10.1029/98WR01340>, 1998.
- 972 Callejas-Rodelas, J. Á., Knohl, A., van Ramshorst, J., Mammarella, I., and Markwitz, C.: Comparison between Lower-Cost and Conventional  
 973 Eddy Covariance Setups for CO<sub>2</sub> and Evapotranspiration Measurements above Monocropping and Agroforestry Systems, *Agricultural and*  
 974 *Forest Meteorology*, 354, 110086, <https://doi.org/10.1016/j.agrformet.2024.110086>, 2024.
- 975 Callejas-Rodelas, J. Á., Knohl, A., Mammarella, I., Vesala, T., Peltola, O., and Markwitz, C.: Dataset of the Journal Article "Does In-  
 976 creased Spatial Replication above Heterogeneous Agroforestry Improve the Representativeness of Eddy Covariance Measurements?",  
 977 <https://doi.org/10.5281/ZENODO.14855287>, 2025.
- 978 Chasmer, L., Barr, A., Hopkinson, C., McCaughey, H., Treitz, P., Black, A., and Shashkov, A.: Scaling and Assessment of GPP from MODIS  
 979 Using a Combination of Airborne Lidar and Eddy Covariance Measurements over Jack Pine Forests, *Remote Sensing of Environment*,  
 980 113, 82–93, <https://doi.org/10.1016/j.rse.2008.08.009>, 2009.
- 981 Chen, B., Black, T. A., Coops, N. C., Hilker, T., (Tony) Trofymow, J. A., and Morgenstern, K.: Assessing Tower Flux Footprint Cli-  
 982 matology and Scaling Between Remotely Sensed and Eddy Covariance Measurements, *Boundary-Layer Meteorology*, 130, 137–167,  
 983 <https://doi.org/10.1007/s10546-008-9339-1>, 2009.
- 984 Chen, B., Coops, N. C., Fu, D., Margolis, H. A., Amiro, B. D., Barr, A. G., Black, T. A., Arain, M. A., Bourque, C. P.-A., Flanagan,  
 985 L. B., Lafleur, P. M., McCaughey, J. H., and Wofsy, S. C.: Assessing Eddy-Covariance Flux Tower Location Bias across the Fluxnet-  
 986 Canada Research Network Based on Remote Sensing and Footprint Modelling, *Agricultural and Forest Meteorology*, 151, 87–100,  
 987 <https://doi.org/10.1016/j.agrformet.2010.09.005>, 2011.
- 988 Chen, T. and Guestrin, C.: XGBoost: A Scalable Tree Boosting System, in: *Proceedings of the 22nd ACM SIGKDD International Conference*  
 989 *on Knowledge Discovery and Data Mining*, pp. 785–794, ACM, San Francisco California USA, <https://doi.org/10.1145/2939672.2939785>,  
 990 2016.

991 Chu, H., Baldocchi, D. D., Poindexter, C., Abraha, M., Desai, A. R., Bohrer, G., Arain, M. A., Griffis, T., Blanken, P. D., O'Halloran, T. L.,  
 992 Thomas, R. Q., Zhang, Q., Burns, S. P., Frank, J. M., Christian, D., Brown, S., Black, T. A., Gough, C. M., Law, B. E., Lee, X., Chen,  
 993 J., Reed, D. E., Massman, W. J., Clark, K., Hatfield, J., Prueger, J., Bracho, R., Baker, J. M., and Martin, T. A.: Temporal Dynamics of  
 994 Aerodynamic Canopy Height Derived From Eddy Covariance Momentum Flux Data Across North American Flux Networks, *Geophysical*  
 995 *Research Letters*, 45, 9275–9287, <https://doi.org/10.1029/2018GL079306>, 2018.  
 996 Cunliffe, A. M., Boschetti, F., Clement, R., Sitch, S., Anderson, K., Duman, T., Zhu, S., Schlumpf, M., Litvak, M. E., Brazier, R. E.,  
 997 and Hill, T. C.: Strong Correspondence in Evapotranspiration and Carbon Dioxide Fluxes Between Different Eddy Covariance Sys-  
 998 tems Enables Quantification of Landscape Heterogeneity in Dryland Fluxes, *Journal of Geophysical Research: Biogeosciences*, 127,  
 999 <https://doi.org/10.1029/2021JG006240>, 2022.  
 1000 Cuxart, J., Wrenger, B., Martínez-Villagrasa, D., Reuder, J., Jonassen, M. O., Jiménez, M. A., Lothon, M., Lohou, F., Hartogensis, O.,  
 1001 Dünnermann, J., Conangla, L., and Garai, A.: Estimation of the Advection Effects Induced by Surface Heterogeneities in the Surface  
 1002 Energy Budget, *Atmospheric Chemistry and Physics*, 16, 9489–9504, <https://doi.org/10.5194/acp-16-9489-2016>, 2016.  
 1003 Davis, P., Brown, J. C., Saunders, M., Lanigan, G., Wright, E., Fortune, T., Burke, J., Connolly, J., Jones, M., and Osborne, B.: Assessing  
 1004 the Effects of Agricultural Management Practices on Carbon Fluxes: Spatial Variation and the Need for Replicated Estimates of Net  
 1005 Ecosystem Exchange, *Agricultural and Forest Meteorology*, 150, 564–574, <https://doi.org/10.1016/j.agrformet.2010.01.021>, 2010.  
 1006 DWD: Deutscher Wetterdienst Climatological Means, 2024.  
 1007 Feigenwinter, C., Bernhofer, C., Eichelmann, U., Heinesch, B., Hertel, M., Janous, D., Kolle, O., Lagergren, F., Lindroth, A., Minerbi, S.,  
 1008 Moderow, U., Mölder, M., Montagnani, L., Queck, R., Rebmann, C., Vestin, P., Yernaux, M., Zeri, M., Ziegler, W., and Aubinet, M.:  
 1009 Comparison of Horizontal and Vertical Advective CO<sub>2</sub> Fluxes at Three Forest Sites, *Agricultural and Forest Meteorology*, 148, 12–24,  
 1010 <https://doi.org/10.1016/j.agrformet.2007.08.013>, 2008.  
 1011 Finnigan, J. J., Clement, R., Malhi, Y., Leuning, R., and Cleugh, H.: A Re-Evaluation of Long-Term Flux Measurement Techniques Part I:  
 1012 Averaging and Coordinate Rotation, *Boundary-Layer Meteorology*, 107, 1–48, <https://doi.org/10.1023/A:1021554900225>, 2003.  
 1013 Foken, T., Göckede, M., Mauder, M., Mahrt, L., Amiro, B., and Munger, W.: Post-Field Data Quality Control, in: *Handbook of Mi-*  
 1014 *crometeorology*, edited by Lee, X., Massman, W., and Law, B., vol. 29, pp. 181–208, Kluwer Academic Publishers, Dordrecht,  
 1015 [https://doi.org/10.1007/1-4020-2265-4\\_9](https://doi.org/10.1007/1-4020-2265-4_9), 2005.  
 1016 Garratt, J. R.: The Internal Boundary Layer ? A Review, *Boundary-Layer Meteorology*, 50, 171–203, <https://doi.org/10.1007/BF00120524>,  
 1017 1990.  
 1018 Göckede, M., Markkanen, T., Hasager, C. B., and Foken, T.: Update of a Footprint-Based Approach for the Characterisation of Complex  
 1019 Measurement Sites, *Boundary-Layer Meteorology*, 118, 635–655, <https://doi.org/10.1007/s10546-005-6435-3>, 2006.  
 1020 Griebel, A., Bennett, L. T., Metzen, D., Cleverly, J., Burba, G., and Arndt, S. K.: Effects of Inhomogeneities within the Flux Footprint on  
 1021 the Interpretation of Seasonal, Annual, and Interannual Ecosystem Carbon Exchange, *Agricultural and Forest Meteorology*, 221, 50–60,  
 1022 <https://doi.org/10.1016/j.agrformet.2016.02.002>, 2016.  
 1023 Hersbach, H., Bell, B., Berrisford, P., Biavati, G., Horányi, A., Muñoz Sabater, J., Nicolas, J., Peubey, C., Radu, R., Rozum, I., Schepers,  
 1024 D., Simmons, A., Soci, C., Dee, D., and Thépaut, J.-N.: ERA5 Hourly Data on Single Levels from 1959 to Present. Copernicus Climate  
 1025 Change Service (C3S) Climate Data Store (CDS)., 2023.  
 1026 Higgins, C. W., Katul, G. G., Froidevaux, M., Simeonov, V., and Parlange, M. B.: Are Atmospheric Surface Layer Flows Ergodic?, *Geo-*  
 1027 *physical Research Letters*, 40, 3342–3346, <https://doi.org/10.1002/grl.50642>, 2013.

1028 Hill, T., Chocholek, M., and Clement, R.: The Case for Increasing the Statistical Power of Eddy Covariance Ecosystem Studies: Why, Where  
 1029 and How?, *Global Change Biology*, 23, 2154–2165, <https://doi.org/10.1111/gcb.13547>, 2017.

1030 Hollinger, D. Y. and Richardson, A. D.: Uncertainty in Eddy Covariance Measurements and Its Application to Physiological Models, *Tree*  
 1031 *Physiology*, 25, 873–885, <https://doi.org/10.1093/treephys/25.7.873>, 2005.

1032 Hollinger, D. Y., Aber, J., Dail, B., Davidson, E. A., Goltz, S. M., Hughes, H., Leclerc, M. Y., Lee, J. T., Richardson, A. D., Rodrigues,  
 1033 C., Scott, N., Achuatavari, D., and Walsh, J.: Spatial and Temporal Variability in Forest–Atmosphere CO<sub>2</sub> Exchange, *Global Change*  
 1034 *Biology*, 10, 1689–1706, <https://doi.org/10.1111/j.1365-2486.2004.00847.x>, 2004.

1035 Hollinger, S. E., Bernacchi, C. J., and Meyers, T. P.: Carbon Budget of Mature No-till Ecosystem in North Central Region of the United  
 1036 States, *Agricultural and Forest Meteorology*, 130, 59–69, <https://doi.org/10.1016/j.agrformet.2005.01.005>, 2005.

1037 Hurlbert, S. H.: Pseudoreplication and the Design of Ecological Field Experiments, *Ecological Monographs*, 54, 187–211,  
 1038 <https://doi.org/10.2307/1942661>, 1984.

1039 Ibrom, A., Dellwik, E., Flyvbjerg, H., Jensen, N. O., and Pilegaard, K.: Strong Low-Pass Filtering Effects on Water  
 1040 Vapour Flux Measurements with Closed-Path Eddy Correlation Systems, *Agricultural and Forest Meteorology*, 147, 140–156,  
 1041 <https://doi.org/10.1016/j.agrformet.2007.07.007>, 2007.

1042 Jänicke, C., Goddard, A., Stein, S., Steinmann, H.-H., Lakes, T., Nendel, C., and Müller, D.: Field-Level Land-Use Data Reveal  
 1043 Heterogeneous Crop Sequences with Distinct Regional Differences in Germany, *European Journal of Agronomy*, 141, 126632,  
 1044 <https://doi.org/10.1016/j.eja.2022.126632>, 2022.

1045 Kaimal, J. C. and Finnigan, J. J.: *Atmospheric Boundary Layer Flows: Their Structure and Measurement*, Oxford University Press,  
 1046 <https://doi.org/10.1093/oso/9780195062397.001.0001>, 1994.

1047 Kanzler, M., Böhm, C., Mirck, J., Schmitt, D., and Veste, M.: Microclimate Effects on Evaporation and Winter Wheat (*Triticum Aestivum*  
 1048 L.) Yield within a Temperate Agroforestry System, *Agroforestry Systems*, 93, 1821–1841, <https://doi.org/10.1007/s10457-018-0289-4>,  
 1049 2019.

1050 Kanzler, M., Böhm, C., and Freese, D.: The Development of Soil Organic Carbon under Young Black Locust (*Robinia Pseudoacacia* L.)  
 1051 Trees at a Post-Mining Landscape in Eastern Germany, *New Forests*, 52, 47–68, <https://doi.org/10.1007/s11056-020-09779-1>, 2021.

1052 Katul, G., Hsieh, C.-I., Bowling, D., Clark, K., Shurpali, N., Turnipseed, A., Albertson, J., Tu, K., Hollinger, D., Evans, B., Offerle, B.,  
 1053 Anderson, D., Ellsworth, D., Vogel, C., and Oren, R.: Spatial Variability of Turbulent Fluxes in the Roughness Sublayer of an Even-Aged  
 1054 Pine Forest, *Boundary-Layer Meteorology*, 93, 1–28, <https://doi.org/10.1023/A:1002079602069>, 1999.

1055 Kay, S., Rega, C., Moreno, G., Den Herder, M., Palma, J. H., Borek, R., Crous-Duran, J., Freese, D., Giannitsopoulos, M., Graves,  
 1056 A., Jäger, M., Lamersdorf, N., Memedemin, D., Mosquera-Losada, R., Pantera, A., Paracchini, M. L., Paris, P., Roces-Díaz, J. V.,  
 1057 Rolo, V., Rosati, A., Sandor, M., Smith, J., Szerencsits, E., Varga, A., Viaud, V., Wawer, R., Burgess, P. J., and Herzog, F.: Agro-  
 1058 forestry Creates Carbon Sinks Whilst Enhancing the Environment in Agricultural Landscapes in Europe, *Land Use Policy*, 83, 581–593,  
 1059 <https://doi.org/10.1016/j.landusepol.2019.02.025>, 2019.

1060 Kljun, N., Rotach, M., and Schmid, H.: A Three-Dimensional Backward Lagrangian Footprint Model For A Wide Range Of Boundary-Layer  
 1061 Stratifications, *Boundary-Layer Meteorology*, 103, 205–226, <https://doi.org/10.1023/A:1014556300021>, 2002.

1062 Kljun, N., Calanca, P., Rotach, M. W., and Schmid, H. P.: A Simple Two-Dimensional Parameterisation for Flux Footprint Prediction (FFP),  
 1063 *Geoscientific Model Development*, 8, 3695–3713, <https://doi.org/10.5194/gmd-8-3695-2015>, 2015.

1064 Kutsch, W. L., Liu, C., Hörmann, G., and Herbst, M.: Spatial Heterogeneity of Ecosystem Carbon Fluxes in a Broadleaved Forest in Northern  
 1065 Germany, *Global Change Biology*, 11, 70–88, <https://doi.org/10.1111/j.1365-2486.2004.00884.x>, 2005.



1066 Launiainen, S., Vesala, T., Mölder, M., Mammarella, I., Smolander, S., Rannik, Ü., Kolari, P., Hari, P., Lindroth, A., and Katul, G. G.:  
 1067 Vertical Variability and Effect of Stability on Turbulence Characteristics down to the Floor of a Pine Forest, *Tellus B: Chemical and*  
 1068 *Physical Meteorology*, 59, 919, <https://doi.org/10.1111/j.1600-0889.2007.00313.x>, 2007.

1069 Levy, P., Drewer, J., Jammet, M., Leeson, S., Friborg, T., Skiba, U., and Oijen, M. V.: Inference of Spatial Heterogeneity in Surface  
 1070 Fluxes from Eddy Covariance Data: A Case Study from a Subarctic Mire Ecosystem, *Agricultural and Forest Meteorology*, 280, 107 783,  
 1071 <https://doi.org/10.1016/j.agrformet.2019.107783>, 2020.

1072 Lokupitiya, E., Denning, S., Paustian, K., Baker, I., Schaefer, K., Verma, S., Meyers, T., Bernacchi, C. J., Suyker, A., and Fischer, M.:  
 1073 Incorporation of Crop Phenology in Simple Biosphere Model (SiBcrop) to Improve Land-Atmosphere Carbon Exchanges from Croplands,  
 1074 *Biogeosciences (Online)*, 6, 969–986, <https://doi.org/10.5194/bg-6-969-2009>, 2009.

1075 Lokupitiya, E., Denning, A. S., Schaefer, K., Ricciuto, D., Anderson, R., Arain, M. A., Baker, I., Barr, A. G., Chen, G., Chen, J. M., Ciais,  
 1076 P., Cook, D. R., Dietze, M., El Maayar, M., Fischer, M., Grant, R., Hollinger, D., Izaurrealde, C., Jain, A., Kucharik, C., Li, Z., Liu, S., Li,  
 1077 L., Matamala, R., Peylin, P., Price, D., Running, S. W., Sahoo, A., Sprintsin, M., Suyker, A. E., Tian, H., Tonitto, C., Torn, M., Verbeeck,  
 1078 H., Verma, S. B., and Xue, Y.: Carbon and Energy Fluxes in Cropland Ecosystems: A Model-Data Comparison, *Biogeochemistry*, 129,  
 1079 53–76, <https://doi.org/10.1007/s10533-016-0219-3>, 2016.

1080 Lucas-Moffat, A. M., Schrader, F., Herbst, M., and Brümmer, C.: Multiple Gap-Filling for Eddy Covariance Datasets, *Agricultural and Forest*  
 1081 *Meteorology*, 325, 109 114, <https://doi.org/10.1016/j.agrformet.2022.109114>, 2022.

1082 Mahrt, L. and Bou-Zeid, E.: Non-Stationary Boundary Layers, *Boundary-Layer Meteorology*, 177, 189–204, [https://doi.org/10.1007/s10546-](https://doi.org/10.1007/s10546-020-00533-w)  
 1083 [020-00533-w](https://doi.org/10.1007/s10546-020-00533-w), 2020.

1084 Mammarella, I. ., Kolari, P., Rinne, J. ., Keronen, P., Pumpanen, J. ., and Vesala, T.: Determining the Contribution of Vertical  
 1085 Advection to the Net Ecosystem Exchange at Hyytiälä Forest, Finland, *Tellus B: Chemical and Physical Meteorology*, 59, 900,  
 1086 <https://doi.org/10.1111/j.1600-0889.2007.00306.x>, 2007.

1087 Mammarella, I., Launiainen, S., Gronholm, T., Keronen, P., Pumpanen, J., Rannik, Ü., and Vesala, T.: Relative Humidity Effect on the High-  
 1088 Frequency Attenuation of Water Vapor Flux Measured by a Closed-Path Eddy Covariance System, *Journal of Atmospheric and Oceanic*  
 1089 *Technology*, 26, 1856–1866, <https://doi.org/10.1175/2009JTECHA1179.1>, 2009.

1090 Mammarella, I., Peltola, O., Nordbo, A., Järvi, L., and Rannik, Ü.: Quantifying the Uncertainty of Eddy Covariance Fluxes Due to the  
 1091 Use of Different Software Packages and Combinations of Processing Steps in Two Contrasting Ecosystems, *Atmospheric Measurement*  
 1092 *Techniques*, 9, 4915–4933, <https://doi.org/10.5194/amt-9-4915-2016>, 2016.

1093 Markwitz, C.: Micrometeorological Measurements and Numerical Simulations of Turbulence and Evapotranspiration over Agroforestry,  
 1094 *Doctoral Thesis, Georg-August-University Göttingen*, <https://doi.org/10.53846/goediss-8477>, 2021.

1095 Markwitz, C. and Siebicke, L.: Low-Cost Eddy Covariance: A Case Study of Evapotranspiration over Agroforestry in Germany, *Atmospheric*  
 1096 *Measurement Techniques*, 12, 4677–4696, <https://doi.org/10.5194/amt-12-4677-2019>, 2019.

1097 Markwitz, C., Knohl, A., and Siebicke, L.: Evapotranspiration over Agroforestry Sites in Germany, *Biogeosciences (Online)*, 17, 5183–5208,  
 1098 <https://doi.org/10.5194/bg-17-5183-2020>, 2020.

1099 Mauder, M., Cuntz, M., Drüe, C., Graf, A., Rebmann, C., Schmid, H. P., Schmidt, M., and Steinbrecher, R.: A Strategy for Qual-  
 1100 ity and Uncertainty Assessment of Long-Term Eddy-Covariance Measurements, *Agricultural and Forest Meteorology*, 169, 122–135,  
 1101 <https://doi.org/10.1016/j.agrformet.2012.09.006>, 2013.

1102 Moncrieff, J., Malhi, Y., and Leuning, R.: The Propagation of Errors in Long-Term Measurements of Land-Atmosphere Fluxes of Carbon  
 1103 and Water, *Global Change Biology*, 2, 231–240, <https://doi.org/10.1111/j.1365-2486.1996.tb00075.x>, 1996.

1104 Muñoz-Sabater, J., Dutra, E., Agustí-Panareda, A., Albergel, C., Arduini, G., Balsamo, G., Boussetta, S., Choulga, M., Harrigan, S.,  
 1105 Hersbach, H., Martens, B., Miralles, D. G., Piles, M., Rodríguez-Fernández, N. J., Zsoter, E., Buontempo, C., and Thépaut, J.-  
 1106 N.: ERA5-Land: A State-of-the-Art Global Reanalysis Dataset for Land Applications, *Earth System Science Data*, 13, 4349–4383,  
 1107 <https://doi.org/10.5194/essd-13-4349-2021>, 2021.

1108 Najibnia, S., Koocheki, A., Nassiri, M., and Porsa, H. M.: Water Capture Efficiency, Use Efficiency and Productivity in  
 1109 Sole Cropping and Intercropping of Rapeseed, Bean and Corn, *European Journal of Sustainable Development*, 3, 347–358,  
 1110 <https://doi.org/10.14207/ejsd.2014.v3n4p347>, 2014.

1111 Oren, R., Hsieh, C.-I., Stoy, P., Albertson, J., McCarthy, H. R., Harrell, P., and Katul, G. G.: Estimating the Uncertainty in Annual Net  
 1112 Ecosystem Carbon Exchange: Spatial Variation in Turbulent Fluxes and Sampling Errors in Eddy-Covariance Measurements, *Global  
 1113 Change Biology*, 12, 883–896, <https://doi.org/10.1111/j.1365-2486.2006.01131.x>, 2006.

1114 Papale, D., Reichstein, M., Aubinet, M., Canfora, E., Bernhofer, C., Kutsch, W., Longdoz, B., Rambal, S., Valentini, R., Vesala, T., and  
 1115 Yakir, D.: Towards a Standardized Processing of Net Ecosystem Exchange Measured with Eddy Covariance Technique: Algorithms and  
 1116 Uncertainty Estimation, *Biogeosciences (Online)*, 3, 571–583, <https://doi.org/10.5194/bg-3-571-2006>, 2006.

1117 Peltola, O., Hensen, A., Helfter, C., Beletti Marchesini, L., Bosveld, F. C., Van Den Bulk, W. C. M., Elbers, J. A., Haapanala, S., Holst, J.,  
 1118 Laurila, T., Lindroth, A., Nemitz, E., Röckmann, T., Vermeulen, A. T., and Mammarella, I.: Evaluating the Performance of Commonly  
 1119 Used Gas Analysers for Methane Eddy Covariance Flux Measurements: The InGOS Inter-Comparison Field Experiment, *Biogeosciences  
 1120 (Online)*, 11, 3163–3186, <https://doi.org/10.5194/bg-11-3163-2014>, 2014.

1121 Peltola, O., Hensen, A., Beletti Marchesini, L., Helfter, C., Bosveld, F., Van Den Bulk, W., Haapanala, S., Van Huissteden, J.,  
 1122 Laurila, T., Lindroth, A., Nemitz, E., Röckmann, T., Vermeulen, A., and Mammarella, I.: Studying the Spatial Variability of  
 1123 Methane Flux with Five Eddy Covariance Towers of Varying Height, *Agricultural and Forest Meteorology*, 214–215, 456–472,  
 1124 <https://doi.org/10.1016/j.agrformet.2015.09.007>, 2015.

1125 Pohanková, E., Hlavinka, P., Orság, M., Takáč, J., Kersebaum, K. C., Gobin, A., and Trnka, M.: Estimating the Water Use Efficiency of Spring  
 1126 Barley Using Crop Models, *The Journal of Agricultural Science*, 156, 628–644, <https://doi.org/10.1017/S0021859618000060>, 2018.

1127 Prabha, T. V., Leclerc, M. Y., and Baldocchi, D.: Comparison of In-Canopy Flux Footprints between Large-Eddy Simulation and the La-  
 1128 grangian Simulation, *Journal of Applied Meteorology and Climatology*, 47, 2115–2128, <https://doi.org/10.1175/2008jamc1814.1>, 2008.

1129 Quandt, A., Neufeldt, H., and Gorman, K.: Climate Change Adaptation through Agroforestry: Opportunities and Gaps, *Current Opinion in  
 1130 Environmental Sustainability*, 60, 101 244, <https://doi.org/10.1016/j.cosust.2022.101244>, 2023.

1131 Ran, Y., Li, X., Sun, R., Kljun, N., Zhang, L., Wang, X., and Zhu, G.: Spatial Representativeness and Uncertainty of Eddy Covariance Carbon  
 1132 Flux Measurements for Upscaling Net Ecosystem Productivity to the Grid Scale, *Agricultural and Forest Meteorology*, 230–231, 114–127,  
 1133 <https://doi.org/10.1016/j.agrformet.2016.05.008>, 2016.

1134 Rannik, Ü. and Vesala, T.: Autoregressive Filtering versus Linear Detrending in Estimation of Fluxes by the Eddy Covariance Method,  
 1135 *Boundary-Layer Meteorology*, 91, 259–280, <https://doi.org/10.1023/A:1001840416858>, 1999.

1136 Rannik, Ü., Kolari, P., Vesala, T., and Hari, P.: Uncertainties in Measurement and Modelling of Net Ecosystem Exchange of a Forest,  
 1137 *Agricultural and Forest Meteorology*, 138, 244–257, <https://doi.org/10.1016/j.agrformet.2006.05.007>, 2006.

1138 Reichstein, M., Falge, E., Baldocchi, D., Papale, D., Aubinet, M., Berbigier, P., Bernhofer, C., Buchmann, N., Gilmanov, T., Granier, A.,  
 1139 Grünwald, T., Havránková, K., Ilvesniemi, H., Janous, D., Knohl, A., Laurila, T., Lohila, A., Loustau, D., Matteucci, G., Meyers, T.,  
 1140 Miglietta, F., Ourcival, J.-M., Pumpanen, J., Rambal, S., Rotenberg, E., Sanz, M., Tenhunen, J., Seufert, G., Vaccari, F., Vesala, T., Yakir,

1141 D., and Valentini, R.: On the Separation of Net Ecosystem Exchange into Assimilation and Ecosystem Respiration: Review and Improved  
 1142 Algorithm, *Global Change Biology*, 11, 1424–1439, <https://doi.org/10.1111/j.1365-2486.2005.001002.x>, 2005.

1143 Richardson, A. D. and Hollinger, D. Y.: A Method to Estimate the Additional Uncertainty in Gap-Filled NEE Resulting from Long Gaps in  
 1144 the CO<sub>2</sub> Flux Record, *Agricultural and Forest Meteorology*, 147, 199–208, <https://doi.org/10.1016/j.agrformet.2007.06.004>, 2007.

1145 Richardson, A. D., Hollinger, D. Y., Burba, G. G., Davis, K. J., Flanagan, L. B., Katul, G. G., William Munger, J., Ricciuto, D. M., Stoy,  
 1146 P. C., Suyker, A. E., Verma, S. B., and Wofsy, S. C.: A Multi-Site Analysis of Random Error in Tower-Based Measurements of Carbon  
 1147 and Energy Fluxes, *Agricultural and Forest Meteorology*, 136, 1–18, <https://doi.org/10.1016/j.agrformet.2006.01.007>, 2006.

1148 Sabbatini, S., Mammarella, I., Arriga, N., Fratini, G., Graf, A., Hörtnagl, L., Ibrom, A., Longdoz, B., Mauder, M., Merbold, L., Metzger, S.,  
 1149 Montagnani, L., Pitacco, A., Rebmann, C., Sedláč, P., Šigut, L., Vitale, D., and Papale, D.: Eddy Covariance Raw Data Processing for  
 1150 CO<sub>2</sub> and Energy Fluxes Calculation at ICOS Ecosystem Stations, *International Agrophysics*, 32, 495–515, [https://doi.org/10.1515/intag-](https://doi.org/10.1515/intag-2017-0043)  
 1151 2017-0043, 2018.

1152 Soegaard, H.: Carbon Dioxide Exchange over Agricultural Landscape Using Eddy Correlation and Footprint Modelling, *Agricultural and*  
 1153 *Forest Meteorology*, 114, 153–173, [https://doi.org/10.1016/S0168-1923\(02\)00177-6](https://doi.org/10.1016/S0168-1923(02)00177-6), 2003.

1154 Stoy, P. C., Chu, H., Dahl, E., Cala, D. S., Shveytser, V., Wiesner, S., Desai, A. R., and Novick, K. A.: The Global Distribution of Paired  
 1155 Eddy Covariance Towers, <https://doi.org/10.1101/2023.03.03.530958>, 2023.

1156 Sun, F., Roderick, M. L., Farquhar, G. D., Lim, W. H., Zhang, Y., Bennett, N., and Roxburgh, S. H.: Partitioning the Variance between Space  
 1157 and Time, *Geophysical Research Letters*, 37, 2010GL043 323, <https://doi.org/10.1029/2010GL043323>, 2010.

1158 Trouwloon, D., Streck, C., Chagas, T., and Martinus, G.: Understanding the Use of Carbon Credits by Companies: A Review of the Defining  
 1159 Elements of Corporate Climate Claims, *Global Challenges*, 7, 2200 158, <https://doi.org/10.1002/gch2.202200158>, 2023.

1160 van Ramshorst, J. G. V., Siebicke, L., Baumeister, M., Moyano, F. E., Knohl, A., and Markwitz, C.: Reducing Wind Erosion through  
 1161 Agroforestry: A Case Study Using Large Eddy Simulations, *Sustainability*, 14, 13 372, <https://doi.org/10.3390/su142013372>, 2022.

1162 van Ramshorst, J. G. V., Knohl, A., Callejas-Rodelas, J. Á., Clement, R., Hill, T. C., Siebicke, L., and Markwitz, C.: Lower-Cost Eddy  
 1163 Covariance for CO<sub>2</sub> and H<sub>2</sub>O Fluxes over Grassland and Agroforestry, <https://doi.org/10.5194/amt-2024-30>, 2024.

1164 Vekuri, H., Tuovinen, J.-P., Kulmala, L., Papale, D., Kolari, P., Aurela, M., Laurila, T., Liski, J., and Lohila, A.: A Widely-  
 1165 Used Eddy Covariance Gap-Filling Method Creates Systematic Bias in Carbon Balance Estimates, *Scientific Reports*, 13, 1720,  
 1166 <https://doi.org/10.1038/s41598-023-28827-2>, 2023.

1167 Veldkamp, E., Schmidt, M., Markwitz, C., Beule, L., Beuschel, R., Biertümpfel, A., Bischel, X., Duan, X., Gerjets, R., Göbel, L., Graß, R.,  
 1168 Guerra, V., Heinlein, F., Komainda, M., Langhof, M., Luo, J., Potthoff, M., Van Ramshorst, J. G. V., Rudolf, C., Seserman, D.-M., Shao,  
 1169 G., Siebicke, L., Svoboda, N., Swieter, A., Carminati, A., Freese, D., Graf, T., Greef, J. M., Isselstein, J., Jansen, M., Karlovsky, P., Knohl,  
 1170 A., Lamersdorf, N., Priesack, E., Wachendorf, C., Wachendorf, M., and Corre, M. D.: Multifunctionality of Temperate Alley-Cropping  
 1171 Agroforestry Outperforms Open Cropland and Grassland, *Communications Earth & Environment*, 4, 20, [https://doi.org/10.1038/s43247-](https://doi.org/10.1038/s43247-023-00680-1)  
 1172 023-00680-1, 2023.

1173 Vesala, T., Kljun, N., Rannik, Ü., Rinne, J., Sogachev, A., Markkanen, T., Sabelfeld, K., Foken, Th., and Leclerc, M.: Flux and Concentration  
 1174 Footprint Modelling: State of the Art, *Environmental Pollution*, 152, 653–666, <https://doi.org/10.1016/j.envpol.2007.06.070>, 2008.

1175 Vuichard, N. and Papale, D.: Filling the Gaps in Meteorological Continuous Data Measured at FLUXNET Sites with ERA-Interim Reanaly-  
 1176 sis, *Earth System Science Data*, 7, 157–171, <https://doi.org/10.5194/essd-7-157-2015>, 2015.

1177 Wang, H., Jia, G., Zhang, A., and Miao, C.: Assessment of Spatial Representativeness of Eddy Covariance Flux Data from Flux Tower to  
 1178 Regional Grid, *Remote Sensing*, 8, 742, <https://doi.org/10.3390/rs8090742>, 2016.

1179 Wilczak, J. M., Oncley, S. P., and Stage, S. A.: Sonic Anemometer Tilt Correction Algorithms, *Boundary-Layer Meteorology*, 99, 127–150,  
1180 <https://doi.org/10.1023/A:1018966204465>, 2001.

1181 Winck, B. R., Bloor, J. M. G., and Klumpp, K.: Eighteen Years of Upland Grassland Carbon Flux Data: Reference Datasets, Processing, and  
1182 Gap-Filling Procedure, *Scientific Data*, 10, 311, <https://doi.org/10.1038/s41597-023-02221-z>, 2023.

1183 Wohlfahrt, G., Hörtnagl, L., Hammerle, A., Graus, M., and Hansel, A.: Measuring Eddy Covariance Fluxes of Ozone with a Slow-Response  
1184 Analyser, *Atmospheric Environment*, 43, 4570–4576, <https://doi.org/10.1016/j.atmosenv.2009.06.031>, 2009.

1185 Wutzler, T., Lucas-Moffat, A., Migliavacca, M., Knauer, J., Sickel, K., Šigut, L., Menzer, O., and Reichstein, M.: Basic and Extensible  
1186 Post-Processing of Eddy Covariance Flux Data with REddyProc, *Biogeosciences (Online)*, 15, 5015–5030, [https://doi.org/10.5194/bg-15-](https://doi.org/10.5194/bg-15-5015-2018)  
1187 5015-2018, 2018.